Nonlinear Dyn (2017) 90:1277–1299
DOI 10.1007/s11071-017-3726-4

ORIGINAL PAPER

Coexistence of single- and multi-scroll chaotic orbits in a single-link flexible joint robot manipulator with stable spiral and index-4 spiral repellor types of equilibria

Jay Prakash Singh · K. Lochan · Nikolay V. Kuznetsov · B. K. Roy

Received: 19 February 2017 / Accepted: 4 August 2017 / Published online: 18 August 2017

Abstract This paper reports various chaotic phenomena that occur in a single-link flexible joint (SLFJ) robot manipulator. Four different cases along with subcases are considered here to show different types of chaotic behaviour in a flexible manipulator dynamics. In the first three cases, a partial state feedback as joint velocity and motor rotor velocity feedback is considered, and the resultant autonomous dynamics is considered for analyses. In the fourth case, the manipulator dynamics is considered as a non-autonomous system. The system has (1) one stable spiral and one saddle-node foci, (2) two saddle-node foci and (3) one marginally stable nature of equilibrium points. We found single- and multi-scroll chaotic orbits in these cases. However, with the motor rotor velocity feedback, the system has two unstable equilibria. One of them has an index-4 spiral repellor. In the non-autonomous case, the SLFJ robot manipulator system has an inverse crisis route to chaos and exhibits (1) transient chaos with a stable limit cycle and (2) chaotic behaviour. In all the four cases, the SLFJ manipulator dynamics exhibits coexistence of chaotic orbits, i.e. multi-stability. The various dynamical behaviours of the system are analysed using available methods like phase portrait, Lyapunov spectrum, instantaneous phase plot, Poincaré map, parameter space, bifurcation diagram, 0–1 test and frequency spectrum plot. The MATLAB simulation results support various claims made about the system. These claims are further confirmed and validated by circuit implementation using NI Multisim.

Keywords Chaos in a single-link flexible joint · Multi-scroll · Stable and unstable equilibria · Bifurcation diagram · Lyapunov spectrum · Non-autonomous system · Transient chaos · Coexistence of chaotic orbits (i.e. multi-stability)

J. P. Singh (✉) · K. Lochan · B. K. Roy
Department of EE, National Institute of Technology Silchar, Silchar, Assam 788010, India
e-mail: jayprakash1261@gmail.com

K. Lochan
e-mail: lochan.nits@gmail.com

B. K. Roy
e-mail: bkrnits@gmail.com

N. V. Kuznetsov
Faculty of Mathematics and Mechanics, Saint-Petersburg State University, Saint-Petersburg, Russia 198504
e-mail: nkuznetsov239@gmail.com

N. V. Kuznetsov
Department of Mathematical Information Technology, University of Jyväkylä, 40014 Kokkola, Finland

1 Introduction

The performance and desired operations of an electromechanical system depend on the dynamics and stability analyses of its mathematical model. An improper choice of a control torque causes an irregular oscillation in the response of a system. One of such irregular nature of oscillations is known as chaotic phenomenon [1–5]. The chaotic behaviour appears in a deterministic

Table 1 Analyses of the available literature on chaotic behaviour in some flexible manipulator and flexible beam

Category of papers	Sub-classification/remarks	References of papers
Synchronisation of SLFJ with chaotic gyroscope for chaotic behaviour		[46–48]
Dynamical analyses	Finding of chaotic behaviour:	
	Dynamical analyses in a slender beam	[39–42]
	Finding of chaotic behaviour in a cantilever beam	[32–37]
	Chaos control in a spatially redundant manipulator with flexible link	[31]
	Chaos in a three-beam structure with attached mass and three-mode interactions	[49]
	Chaotic behaviour in a four-bar mechanism having revolute joint	[50]
	Chaotic behaviour in a single-link Cartesian manipulator	[24,49–51]
	Bifurcation analysis and chaotic behaviour in an SLFJ robot manipulator	This work
	Coexistence of single- and multi-scroll chaotic attractors in an SLFJ robot manipulator	This work
	A SLFJ robot manipulator with index-4 spiral repellor type of equilibria	This work

nonlinear system and is highly sensitive to initial conditions. Advancement and development of chaos theory increase the applicability of chaotic systems. Recently, chaotic systems are used in many applications like biomedical, artificial neural network, secure communications, information technology, robotics, image processing and cryptography [6–8]. Chaotic and hyperchaotic systems are classified as either self-excited attractors or hidden attractors chaotic systems [9–16]. In the case of hidden attractor chaotic systems, its basin of attraction does not intersect with small open neighbourhood of equilibrium points of the system [9–14].

Chaotic phenomena are observed in many electromechanical and electronics systems like permanent magnet synchronous motor [17], reluctance motor drive [18], permanent magnet DC motor drive [19], electrical solar drive system [20], brushless DC motor [21], drilling system with induction motor [22], rigid robot manipulator [23–25], Duffing oscillator [26] and pendulum [27]. Hidden attractors with and without equilibria are seen in translational oscillator–rotational actuator, drilling system actuated by a DC motor and drilling system actuated by an induction motor [28]. Motivated by the above discussion on the chaotic behaviour of electromechanical systems, this paper explores the possibility of generation of various chaotic behaviours in a single-link flexible joint robot manipulator using different choices of control input. The study of chaotic behaviours in an electromechanical system may be desirable in some cases [27,28]. Application of chaotic dynamics in a robot is categorically discussed in [29]. The potential applications of chaos in robot research are a chaotic mobile robot, chaotic optimisation algorithm and chaos in bipedal locomotion [29]. Another important application is the use of anti-control to show different complex dynamical behaviours in robot dynamics [23,24]. Flexible manipulators (FMs) are used in many fields like industry, medical and defence [30]. FMs are more used in industrial applications in comparison with their rigid counterparts. Some advantages of FMs are low power consumption and light weight [30]. Some challenges are also associated with flexible manipulators like under-actuation, non-collocation, non-minimum phase and nonlinearity [30] which create problems in the controller design. Nonlinear oscillation and chaotic behaviours of some flexible links [31], cantilever beam [32–37], elastic linkage mechanism [38], a slender beam [39–42], spatially redundant manipulator [31], etc., are reported in the literature. The literature available on chaotic behaviour in some flexible beams and flexible manipulators is listed in Table 1. It is observed from Table 1 and according to the best of authors' knowledge, no paper is reported in the literature on the generation and analyses of chaotic behaviours in a single-link flexible joint manipulator.

Recently, chaotic/hyperchaotic systems are used in many directions like control [23], anti-control [50],

Table 2 Classification of 4-D chaotic/hyperchaotic systems based on the nature of equilibria

Characteristics of equilibrium points	Reference of paper
No equilibrium	[54,55]
One unstable	[56]
One stable	[57]
Two stable	[58]
Two unstable	[59]
One stable one unstable	This work
Three stable	
Three unstable	[60]
Two stable one unstable	[61]
Four unstable	[62]
Two stable two unstable	
Three unstable one stable	
Many stable equilibria	[64]
Many equilibria	[64,65,79]

synchronisation [21], optimisation of Lyapunov exponents [52,53] and applications [6–8]. Above-said research directions are discussed and analysed in fractional order also [43–45]. Equilibrium point plays an important role in the classification of chaotic systems. In the past decade, many chaotic or hyperchaotic systems have been reported with different natures of equilibrium points. A list of classification of 4-D chaotic or hyperchaotic systems based on the nature of equilibrium points (EPs) is given in Table 2.

There may be many other papers related to the classifications which are given in Table 2. We have searched and ensured that all different natures of EPs are reflected in the list. It is clear from Table 2 that no 4-D chaotic system is reported with one stable and one unstable nature of equilibria. This paper reports a 4-D SLFJ robot manipulator chaotic system which has one unstable and one stable nature of equilibrium points. This paper reports various chaotic behaviours in a single-link flexible joint robot manipulator. The chaotic behaviours are shown using different choices of control input. Such choice of control inputs for dynamical analyses and generation of chaos in rigid manipulators can be seen in references like in [66,67]. Moreover, in the literature of hyperchaotic/chaotic systems, trigonometric functions are used for many purposes like references [71,72] use the trigonometric sin function as a feedback control to generate hyperchaotic systems with the desired number of positive Lyapunov exponents. Multi-scroll chaotic attractors are generated using a trigonometric sin function in [73–75]. A new approach for generating chaotic phenomenon called 'chaos entanglement' is proposed in [76] using trigonometric sin function. Different cases/subcases are considered here using different choices of control inputs with various trigonometric functions. These cases are as given below along with their behaviours:

1. A joint velocity feedback control ($u = a \cos(2\pi x_2)$). Three subcases are considered here. These are
   i. $a = 3$ generates a single-scroll chaotic attractor and the system has one stable and one unstable equilibrium points,
   ii. $a = 4$ generates multi-scroll chaotic attractors and system has one stable and one unstable equilibrium points,
   iii. $a = 5$ generates multi-scroll chaotic attractors and the system has one marginally stable equilibrium point. Thus, in this subcase, the system may have hidden chaotic orbits [9–14].
2. A joint velocity feedback control ($u = 3\cos(x_2 - c)\tanh(100(x_2 - d))$); It exhibits single-scroll chaotic attractor; parameter space between parameter '$c - d$' shows various behaviours like chaotic, periodic, stable and quasi-periodic. The system has two saddle-node foci.
3. A motor rotor velocity feedback control ($u = a\cos(2\pi x_4 - c)$); It generates a single-scroll chaotic attractor and the system has index-4 spiral repellor. The bifurcation diagram for parameter a reveals both chaotic and periodic behaviours of the system.
4. An open-loop control as a non-autonomous system ($u = a\cos(2\pi f t)$). This case is divided into two subcases.
   A. $a = 2.29$ generates transient chaos with a stable limit cycle at the steady state. Here, the system has an inverse crisis route to chaos,
   B. $a = 4$ generates chaotic behaviours; the bifurcation diagram for parameter a results in chaos and periodic behaviours for a wide range of values of parameter a.

In all cases, the SLFJ manipulator dynamics exhibits coexistence of chaotic attractors i.e. multi-stability. The complex dynamical behaviours as stated above are analysed using various tools like phase portrait, time series plot, Poincaré maps, 0–1 test, Lyapunov exponents, Lyapunov spectrum, bifurcation diagram, instantaneous phase and frequency spectrum. For the first and second cases, Lyapunov spectrum (for a range of parameter value) is calculated. For some other cases, Lyapunov exponents (for a particular value of the parameter) are given in the paper. An application for small signal detection is shown by the non-autonomous SLFJ robot manipulator dynamics.

The novelty and contributions of the paper are summarised as follows:

1. The paper reports various types of chaotic behaviours in a single-link flexible joint (SLFJ) robot manipulator,
2. The paper adds a new class of equilibria having one stable and one unstable equilibrium points of a 4-D chaotic system,
3. The system
   i. has single- and multi-scroll chaotic attractors,
   ii. depicts multi-stability, i.e. coexistence of chaotic attractors under various conditions,
   iii. has one stable and one unstable equilibrium points,
   iv. has index-4 spiral repellor types of equilibrium point,
4. Bifurcation analysis of the SLFM dynamics reveals that:
   i. it has an inverse crisis route to chaos,
   ii. it exhibits transient chaos followed by a stable limit cycle.

Remaining part of the paper is organised as follows. Section 2 describes the dynamics of a single-link flexible joint robot manipulator. Chaotic behaviour in an autonomous SLFJ manipulator using a partial joint velocity feedback control is presented in Sects. 3 and 4. Section 5 represents the chaotic behaviour in the system using a partial motor rotor velocity feedback control. Section 6 describes the chaotic behaviour in the non-autonomous SLFJ robot manipulator. The circuit design and simulation using NI Multisim of the SLFJ robot manipulator are discussed in Sect. 7. An application of the non-autonomous SLFJ robot manipulator for small signal detection is given in Sect. 8. Conclusions of the paper are presented in Sect. 9.

2 Description of a single-link flexible joint (SLFJ) robot manipulator dynamics

The standard dynamic model of a n-link rigid robot manipulator can be written as [68,69]

$$(D(q)+J)\ddot{q}+C(q,\dot{q})\dot{q}+g(q)=\tau, \tag{1}$$

where $q \in R^n$ is the joint angles, $D(q) \in R^{n\times n}$ is the inertia matrix, J is the actuator inertia matrix, $g(q)$ is the gravitational terms, $C(q,\dot{q})$ is the centrifugal and coriolis terms, $\tau \in R^n$ is the input torque. The matrix $D(q)$ is symmetric and $D(q)-2C(q,\dot{q})$ is skew symmetric. For a flexible joint, the degree of freedom of the system increases. Suppose, θ and α are the link angle and motor angle, respectively, and k is a diagonal stiffness constants matrix. For simplicity, we assume that all the joint stiffness constants are same, so in such a case, k may be considered as a scalar. Considering the above facts, the dynamic model (1) for a flexible joint manipulator can be modified as:

$$D(\theta)\ddot{\theta}+C\left(\theta,\dot{\theta}\right)\dot{\theta}+g(\theta)+k(\theta-\alpha)=0. \tag{2}$$

$$J\ddot{\alpha}-k(\theta-\alpha)=u. \tag{3}$$

The model of a flexible joint robot manipulator which is given in (2) and (3) reduces to (1) as the joint stiffness k tends to infinity [70]. For a single-link flexible joint manipulator, Eqs. (2) and (3) reduce to (4). The schematic model of a single-link flexible joint robot arm is shown in Fig. 1. The symbols and notations used in Fig. 1 are defined in Table 3. The motion equations of a single-link flexible joint robot manipulator are described as [70,77]:

$$\begin{cases} I\ddot{\theta}+mgl\sin(\theta)+k(\theta-\alpha)=0 \\ J\ddot{\alpha}+B\dot{\alpha}-k(\theta-\alpha)=u. \end{cases} \tag{4}$$

Equation (4) can be rearranged as:

$$\begin{cases} \ddot{\theta}=-\frac{mgl}{I}sin(\theta)-\frac{k}{I}(\theta-\alpha)=0 \\ \ddot{\alpha}=-\frac{B}{J}\dot{\alpha}+\frac{k}{J}(\theta-\alpha)+\frac{1}{J}u, \end{cases} \tag{5}$$

where I, J, B, mgl, k, θ and α are the link inertia, rotor inertia, rotor friction, nominal load, joint stiffness, link position and motor rotor position, respectively. The

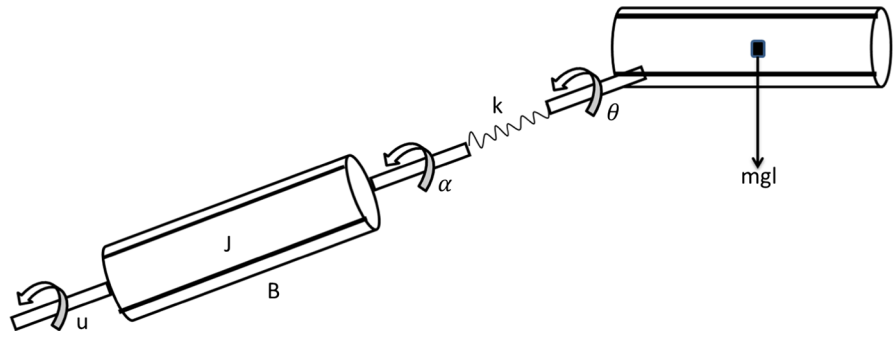

Fig. 1 Schematic of a single-link flexible joint robot arm

Table 3 Parameters of system (4) and their value [77]

Symbol and its description	Value
I : link inertia	1 kgm^2
J: rotor inertia	0.3 kgm^2
B: rotor friction	0.102 kgm^2/s
mgl : nominal payload	5 Nm
k : joint stiffness	100.2 Nm

value of the parameters is given in Table 3. Considering $p_1 = \frac{mgl}{I}$, $p_2 = \frac{k}{I}$, $p_3 = \frac{k}{J}$, $p_4 = \frac{B}{J}$, $p_5 = \frac{1}{J}$, $x_1 = \theta$, $x_2 = \dot{\theta}$, $x_3 = \alpha$, $x_4 = \dot{\alpha}$, the SLFJ manipulator dynamics (5) can be written as:

$$\begin{cases} \dot{x}_1 = x_2 \\ \dot{x}_2 = -p_1 \sin(x_1) - p_2(x_1 - x_3) \\ \dot{x}_3 = x_4 \\ \dot{x}_4 = p_3(x_1 - x_3) - p_4 x_4 + p_5 u, \end{cases} \tag{6}$$

where x_1, x_2, x_3 and x_4 are the link position, link angular velocity, motor rotor position and motor rotor angular velocity, respectively, and u is the control input. The Jacobian matrix of system (6) when $u = 0$ can be written as

$$J_1 = \begin{bmatrix} 0 & 1 & 0 & 0 \\ -p_1 \cos(x_1) - p_2 & 0 & p_2 & 0 \\ 0 & 0 & 0 & 1 \\ p_3 & 0 & -p_3 & -p_4 \end{bmatrix}. \tag{7}$$

The rank of the Jacobian matrix (7) is four. In next two sections, input u is considered as a partial state feedback of link velocity and motor velocity. Thus, the closed-loop system behaves as an autonomous system. In these cases, system (6) is termed as autonomous. When the control input u is considered as function of time t, the open-loop system (6) is termed as non-autonomous.

3 Case 1: Single- and multi-scroll chaotic attractors in an SLFJ manipulator dynamics using a partial joint velocity feedback control ($u = a\cos(2\pi x_2)$)

Here, three different subcases are considered with different control input in (6). Control torque is selected as a partial state feedback of joint velocity. The dynamics of the SLFJ manipulator is considered as in (8) for the three subcases in this section:

$$\begin{cases} \dot{x}_1 = x_2 \\ \dot{x}_2 = -p_1 \sin(x_1) - p_2(x_1 - x_3) \\ \dot{x}_3 = x_4 \\ \dot{x}_4 = p_3(x_1 - x_3) - p_4 x_4 + p_5\, a \cos(2\pi x_2)\,. \end{cases} \tag{8}$$

In system (8), the amplitude of the control input, a, is considered as a bifurcation parameter. With the variation of this parameter a, the SLFJ manipulator dynamics depicts different behaviours. Such analyses are presented in next three subsections. The Jacobian matrix of system (8) can be described as

$$J_2 = \begin{bmatrix} 0 & 1 & 0 & 0 \\ -p_1 \cos(x_1) - p_2 & 0 & p_2 & 0 \\ 0 & 0 & 0 & 1 \\ p_3 & -p_5 a\, 2\pi\, sin(2\pi x_2) & -p_3 & -p_4 \end{bmatrix}. \tag{9}$$

It is seen from (9) that with a variation of parameter a and keeping other parameters of the system fixed, the natures of eigenvalues of system (8) change.

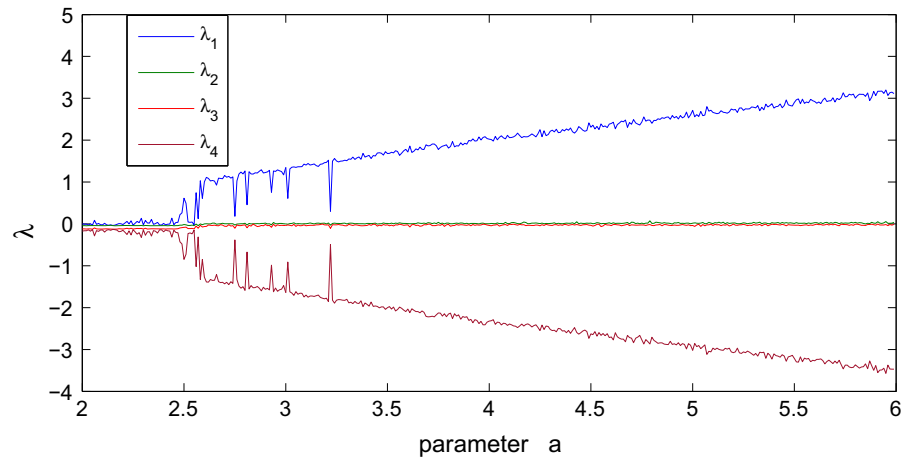

Fig. 2 Lyapunov spectrum of system (8) with the changes in the amplitude of control input with initial conditions $x\,(0) = (0.8,\ 0.001,\ 0.1,\ 0.001)^{\mathrm{T}}$

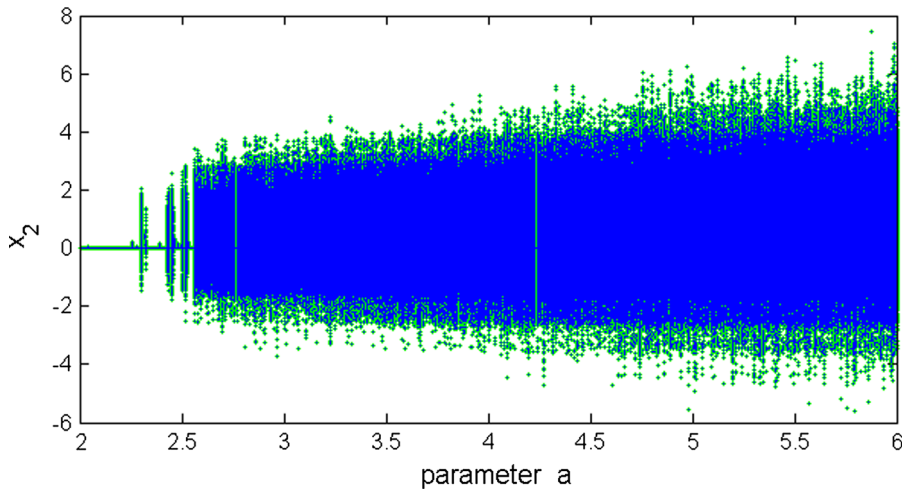

Fig. 3 Bifurcation diagram of system (8) with the changes in parameter a with initial conditions $x\,(0) = (0.8,\ 0.001,\ 0.1,\ 0.001)^{\mathrm{T}}$

The Lyapunov spectrum and the bifurcation diagram of system (8) with variation in parameter a but keeping others fixed are calculated to show the various dynamical behaviours of system (8). The Lyapunov spectrum is calculated by finding Lyapunov exponents with $x\,(0) = (0.8,\ 0.001,\ 0.1,\ 0.001)^{\mathrm{T}}$ initial conditions and by using Wolf algorithm [78] in MATLAB 14-a simulation environment. The Lyapunov spectrum and bifurcation diagram of system (8) with the variation of parameter a are shown in Figs. 2 and 3, respectively. The Lyapunov spectrum and the bifurcation diagram are plotted by keeping $x(0)$ fixed and varying one parameter, in a range, of the system. It helps us to find a correlation of conclusion from these two plots. Positive Lyapunov exponents usually indicate chaos [78–80]. Thus, it is noted from Fig. 2 that the system has chaotic behaviour [79]. The chaotic behaviour of the system is also validated from the bifurcation diagram, shown in Fig. 3. It is observed from Figs. 2 and 3 that system (8) has chaotic behaviour for $a > 2.451$ and has periodic behaviour for low value of the parameter a. It is also apparent that the system has a large range of parameter for chaotic behaviour.

3.1 Case 1(I): Control input ($u = 3\cos(2\pi x_2)$)

The equilibrium points and eigenvalues of Case1(I) of system (8) are given in Table 4. It is observable from Table 4 that the system has one stable and one unstable equilibrium points. The chaotic orbits of Case1(I) of system (8) are shown in Fig. 4. It is noted from Fig. 4 that the system has single-scroll chaotic orbits. The shape of chaotic orbits remain same irrespective of the observation time. The aperiodic nature of orbits shown in Fig. 4 indicates the chaotic behaviour of the system.

Table 4 Equilibria and their corresponding eigenvalues of Case 1(I) of system (8)

Equilibrium points	Eigenvalues	Nature
$E1 = (0.6435,\ 0,\ 0.6735,\ 0)$	$\lambda_i = (-0.0397 \pm 1.7522\,i,\ -0.13026 \pm 20.85402\,i)$	Stable
$E2 = (2.498,\ 0,\ 2.528,\ 0)$	$\lambda_i = (1.71821,\ -0.131379 \pm 20.80979i)$	Unstable

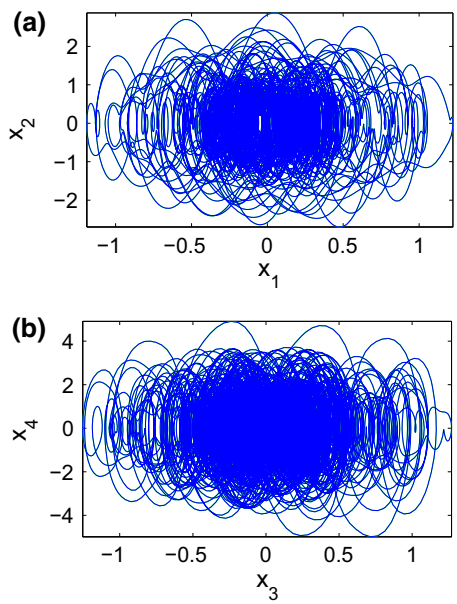

Fig. 4 Chaotic orbits of Case 1(I) of system (8) with $x\,(0) = (0.8,\ 0.001,\ 0.1,\ 0.001)^{\mathrm{T}}$, $\triangle t = 0.01$

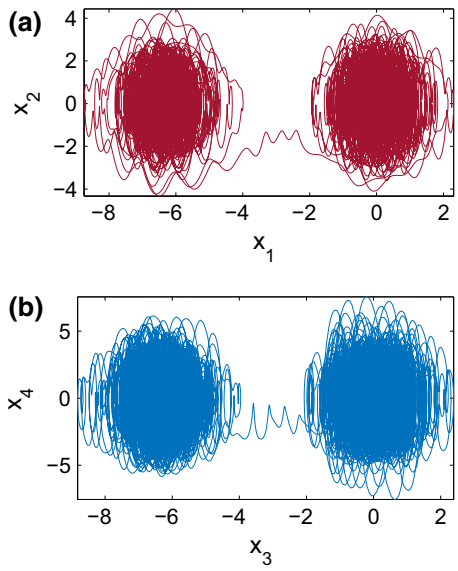

Fig. 5 Two-scroll chaotic orbits in Case 1(II) of system (8) with $x\,(0) = (0.8,\ 0.1,\ 0.1,\ 0.001)^{\mathrm{T}}$, $\triangle t = 0.01$ and $T = 5500$

3.2 Case 1(II): Control input ($u = 4\cos(2\pi x_2)$)

With this control input, the equilibrium points and eigenvalues of system (8) are given in Table 5. It is observed from Table 5 that in Case 1(II) of system (8) has one stable and one unstable nature of equilibrium points. Two-scroll and four-scroll chaotic orbits are observed in Case 1(II) of system (8) with observation time $T = 5500$ time unit and $T = 8200$ time unit, respectively, and are shown in Figs. 5 and 6. In MATLAB, we used time variable in the format like $T = 0 : 0.001 : 1000$. Here, 1000 is termed as the observation time and $\triangle t = 0.001$ is the step size. Here, the unit of time could be in second (s). It is apparent from Figs. 5 and 6 that with the increase in the observation time, the system has increased number of scroll. The Poincaré maps in Case 1(II) of system (8) when $x_1 = 0$ and $x_4 = 0$ are shown in Fig. 7. The random locations of dots in the Poincaré maps and aperiodic behaviour of phase portraits validate the chaotic nature of system (8). The system exhibits various-scroll chaotic orbits with a change in observation time and initial conditions. Some such examples are given in Table 6.

Table 5 Equilibria and their corresponding eigenvalues of Case 1(II) of system (8)

Equilibrium points	Eigenvalues	Nature
$E1 = (0.9272, 0, 0.9672, 0)$	$\lambda_i = (-0.03959 \pm 1.517763\,i,\ -0.130408 \pm 20.848433\,i)$	Stable
$E2 = (2.2142, 0, 2.2542, 0)$	$\lambda_i = (1.482435,\ -1.559951\ \ -0.131242 \pm 20.81525i)$	Unstable

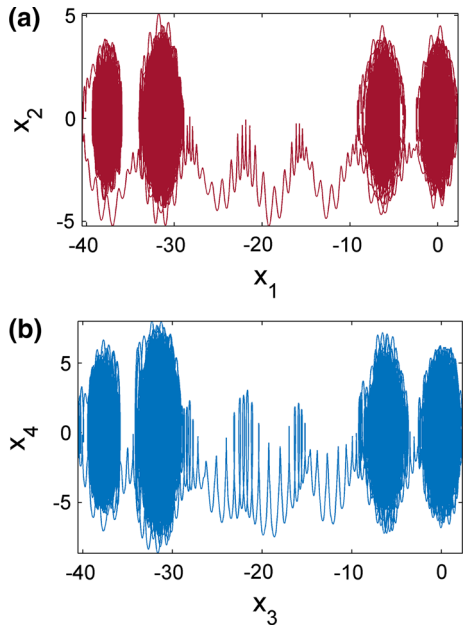

Fig. 6 Four-scroll chaotic orbits in Case 1(II) of system (8) with $x\,(0) = (0.1, 0.1, 0.1, 0.001)^{\mathrm{T}}$, $\triangle t = 0.01$ and $T = 8200$

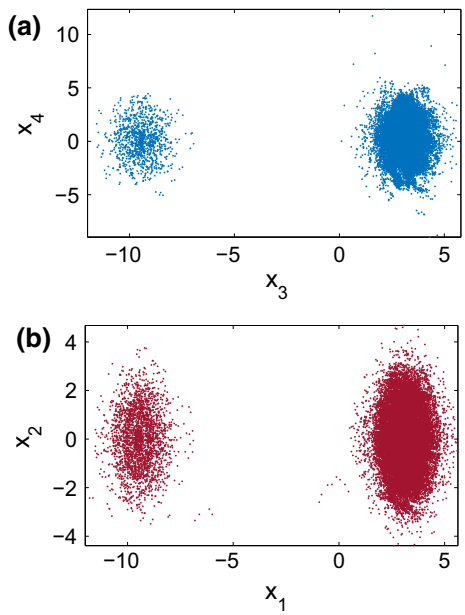

Fig. 7 Poincare maps in Case 1(II) of system (8): **a** across $x_3 - x_4$ when $x_1 = 0$ and **b** across $x_1 - x_2$ when $x_4 = 0$

3.3 Case 1(III): Control input ($u = 5\cos(2\pi x_2)$)

For this case, the equilibrium point and eigenvalues of system (8) when $u = 5\cos(2\pi x_2)$ are given in Table 7.

Table 6 Initial conditions and shape of attractors in Case 1(II) of system (8) with $\triangle t = 0.01$.

Initial conditions	Observation time	Shape
$x\,(0) = (0.1, 0.1, 0.1, 0.001)^{\mathrm{T}}$	$T = 1000$	Single-scroll
$x\,(0) = (0.1, 0.1, 0.1, 0.001)^{\mathrm{T}}$	$T = 2000$	Two-scroll
$x\,(0) = (0.1, 0.1, 0.1, 0.001)^{\mathrm{T}}$	$T = 5000$	Three-scroll
$x\,(0) = (0.1, 0.1, 0.1, 0.001)^{\mathrm{T}}$	$T = 8200$	Four-scroll
$x\,(0) = (0.1, 0.1, 0.1, 0.001)^{\mathrm{T}}$	$T > 8200$	point
$x\,(0) = (0.1, 0.001, 0.1, 0.001)^{\mathrm{T}}$	$T = 2000$	Single-scroll
$x\,(0) = (0.1, 0.001, 0.1, 0.001)^{\mathrm{T}}$	$T = 10000$	Two-scroll
$x\,(0) = (0.8, 0.001, 0.1, 0.001)^{\mathrm{T}}$	$T < 3200$	Single-scroll
$x\,(0) = (0.8, 0.001, 0.1, 0.001)^{\mathrm{T}}$	$T > 3200$	Two-scroll

It is seen from Table 7 that for Case 1(III) of system (8) has only one marginally stable equilibrium point. Since one of the eigenvalues of Case 1(III) of system (8) is zero, thus the Jacobian matrix in this case has rank less than four. Since eigenvalues of the system are marginally stable nature, thus in Case 1(III), the system may have hidden chaotic orbits [57].

The system (Case 1(III)) generates different shapes of various-scroll chaotic orbits depending upon the choice of initial conditions and observation times. Two-scroll and eight-scroll chaotic orbits in Case 1(III) of system (8) are shown in Figs. 8 and 9, respectively. The coexistence of chaotic orbits in Case 1(III) of system (8) is shown in Fig. 10. It is seen from Fig. 10 that system has coexistence of two-scroll and five-scroll chaotic orbits during $1500 < T < 6500$ observation time. Thus, the system exhibits multi-stability with the change in initial conditions. It is also noted from above results in Figs. 8, 9 and 10 that with the increase in observation time, the number of scroll of system (8) increases. Therefore, we can say that the system may have infinite number of scroll at a very large time.

4 Case 2: Single-scroll chaotic attractors in an SLFJ manipulator dynamics using a partial joint velocity feedback control input ($u = 3\cos(x_2 - c)\tanh(100(x_2 - d))$)

In Case 1(II) and Case 1(III), the responses change with an increase in the observation time. In this sec-

Table 7 Equilibria and their corresponding eigenvalues in Case 1(III) of system (8)

Equilibrium points	Eigenvalues	Nature
$E1 = (1.5707,\ 0,\ 1.6207,\ 0)$	$\lambda_i = (0,\ -0.0783447\ -0.130827 \pm 20.831763\, i)$	Marginally stable

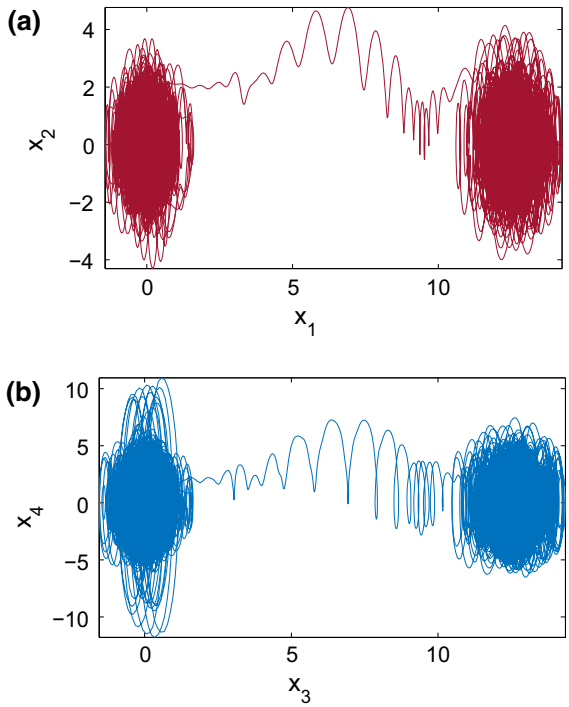

Fig. 8 A two-scroll chaotic orbits for Case 1(III) of system (8) with $x\,(0) = (0.8,\ 0.1,\ 0.1,\ 0.001)^{\mathrm{T}}$, $\triangle t = 0.01$ and $T = 2500$

tion, a piecewise linear term is multiplied with the control input. It is shown that system (8) has single-scroll chaotic orbits irrespective of the observation time. The system dynamics and Jacobian matrix of Case 2 are given in (10) and (11), respectively.

$$\begin{cases} \dot{x}_1 = x_2 \\ \dot{x}_2 = -p_1 \sin(x_1) - p_2\,(x_1 - x_3) \\ \dot{x}_3 = x_4 \\ \dot{x}_4 = p_3\,(x_1 - x_3) - p_4 x_4 + p_5\, a\, cos\,(x_2 - c) \\ \quad \tanh(100\,(x_2 - d)). \end{cases} \tag{10}$$

$$J_3 = \begin{bmatrix} 0 & 1 & 0 & 0 \\ -p_1 \cos(x_1) - p_2 & 0 & p_2 & 0 \\ 0 & 0 & 0 & 1 \\ p_3 & p_5(A) & -p_3 & -p_4 \end{bmatrix} \tag{11}$$

$A = -a\ \cos(x_2 - c)\big(100\tanh(100\,(x_2 - d))^2 - 100\big) - a\,\sin(x_2 - c)\tanh(100\,x_2 - 100\,\mathrm{d})$.

The equilibrium points and eigenvalues of system (10) are given in Table 8. The equilibrium points and eigenvalues of system (10) are calculated with $tanh(...)$ function by using MATLAB 14-a simulation method. It is seen from Table 8 that system (10) has two unstable equilibrium points. The system has single-scroll chaotic orbits with $x\,(0) = (0.5, 0.001, 0.1, 0.001)^{\mathrm{T}}$, $\triangle t = 0.01, a = 3, c = 0.5, d = 0.5$. The chaotic orbits of system (10) with $\triangle t = 0.01,\ c = 0.5,\ d = 0.5$ after ignoring the initial transient parts are shown in Fig. 11. It is observed from Fig. 11 that the system has a bounded chaotic orbits. Here, our analysis says that the number of scrolls of system (10) remains fixed irrespective of the observation time. The parameter space to show the effect of variation of parameters c and d is shown in Fig. 12.

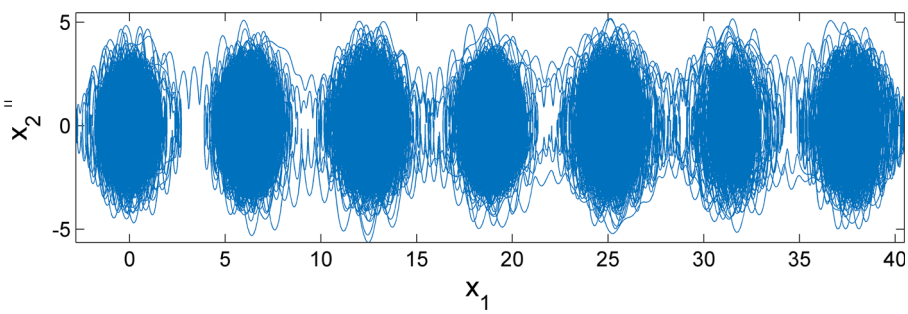

Fig. 9 Seven-scroll chaotic orbits for Case 1(III) of system (8) with $x\,(0) = (0.5,\ 0.001,\ 0.1,\ 0.001)^{\mathrm{T}}$, $\triangle t = 0.01$ and $T = 15000$

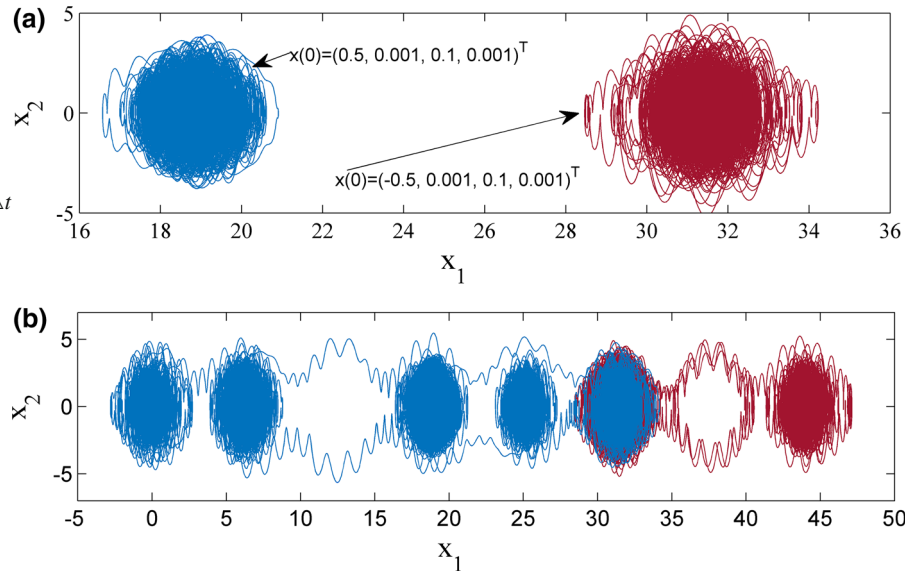

Fig. 10 **a** Coexistence of single-scroll chaotic orbits at $2500 \leq T \leq 3500$ and **b** coexistence of two-scroll and five-scroll chaotic orbits at $1500 < T < 6500$ of system (8) with $x\,(0) = (\pm 0.5,\ 0.1,\ 0.1,\ 0.001)^{\mathrm{T}}$ and $\triangle t$ 0.01 in Case 1(III)

Table 8 Equilibria and their corresponding eigenvalues of system (10) with $c = 0.5,\ d = 0.5$

Equilibrium points	Eigenvalues	Nature
$E1 = (-0.2457,\ 0,\ -0.2579,\ 0)$	$\lambda_i = (0.424 \pm 20.876,\ -0.5947 \mp 1.7036)$	Unstable
$E2 = (3.387,\ 0,\ 3.3752,\ 0)$	$\lambda_i = (1.3139,\ 0.4177 \mp 20.8285,\ -2.4895)$	Unstable

The parameter space of the system for different values of c and d is shown by calculating the Lyapunov exponents. It is seen from Fig. 12 that the SLFJ manipulator dynamics under Case 2 has chaotic, periodic and stable behaviours with different values of c and d.

5 Case 3: Single-scroll chaotic attractors in an SLFJ manipulator dynamics using a partial motor rotor feedback control ($u = a\ \cos(2\pi(x_4 - c))$)

The control input is considered as a partial joint velocity feedback control in Sects. 3 and 4. However, in this section, the motor rotor velocity feedback is considered as a control input. The SLFJ manipulator dynamics is reproduced with $u = a\ cos\ (2\pi\ (x_4 - 0.3))$ in (12).

$$\begin{cases} \dot{x}_1 = x_2 \\ \dot{x}_2 = -p_1 \sin(x_1) - p_2\,(x_1 - x_3) \\ \dot{x}_3 = x_4 \\ \dot{x}_4 = p_3\,(x_1 - x_3) - p_4 x_4 + p_5 a\ cos\ (2\pi(x_4 - 0.3))\,. \end{cases} \tag{12}$$

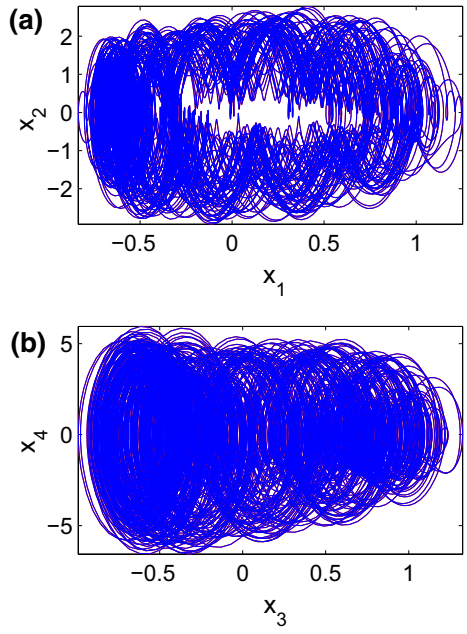

Fig. 11 Chaotic orbits of system (10) with $x\,(0) = (0.5,\ 0.1,\ 0.1,\ 0.001)^{\mathrm{T}}$, $\triangle t = 0.01$ and $T = 500$

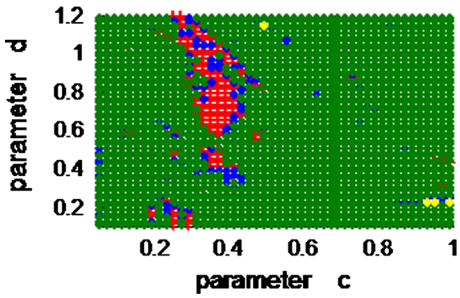

Fig. 12 Parameter space between parameters c and d of system (10) where *red*, *blue*, *green* and *yellow* indicate chaotic, periodic, stable and quasi-periodic behaviours, respectively. (Color figure online)

The Jacobian matrix of system (12) is given in (13).

$$J_4 = \begin{bmatrix} 0 & 1 & 0 & 0 \\ -p_1\cos(x_1) & -p_2 & 0 & p_2 & 0 \\ 0 & 0 & 0 & 1 \\ p_3 & 0 & -p_3 & A \end{bmatrix} \quad (13)$$

where $A = -p_4 - p_5 a\, 2\pi\, sin\,(2\pi(x_4 - 0.3))$.

The equilibrium points and eigenvalues of system (12) are given in Table 9. It is seen from Table 9 that system (12) has two unstable equilibrium points. The equilibrium point $E1$ of system (12) has index-4 spiral repellor which is unique in the literature.

The chaotic orbits of system (12) with $a = 4$, $x\,(0) = (0.5,\ 0.001,\ 0.1,\ 0.001)^{\mathrm{T}}$, $\triangle t = 0.01$, and ignoring the initial transient responses are shown in Fig. 13. The coexistence of chaotic orbits of system (12) with initial conditions $(\pm 0.5,\ 0.001,\ 0.1,\ 0.001)^{\mathrm{T}}$ is shown in Fig. 14. It is noted from Fig. 14 that system (12) has multi-stability with the change in initial conditions. Frequency spectra of x_1 and x_2 signals of system (12) are shown in Fig. 15. Random locations of peaks in the spectra of Fig. 15 indicate the chaotic behaviour of system (12). The bifurcation diagram of system (12) with variation of parameter a is shown in Fig. 16. It is seen from Fig. 16 that system (12) has various behaviours like periodic and chaotic with variation of the amplitude of the control input. It is observed from Fig. 16 that for smaller value of, i.e. $a < 1.7$ and larger value of i.e. $a > 4.98$, system (12) has periodic behaviour.

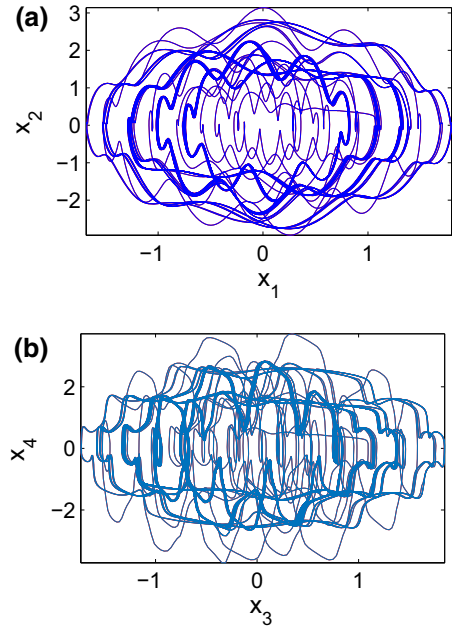

Fig. 13 Chaotic orbits of system (12) with $x\,(0) = (0.5,\ 0.001,\ 0.1,\ 0.001)^{\mathrm{T}}$, $\triangle t = 0.01$ and $T = 500$

6 Case 4: Self-excited attractors in an SLFJ manipulator dynamics using an open-loop control input ($u = a\cos(2\pi f t)$)

In previous sections, joint velocity and motor rotor velocity are considered as a control input u. So, the closed-loop SLFJ manipulator behaves as an autonomous system. In this section, an open-loop control input $u = a\,cos\,(2\pi f t)$ is considered as a function of time t, and thus, the SLFJ manipulator dynamics (6) becomes non-autonomous as described in (14).

Table 9 Equilibria and their corresponding eigenvalues of system (12) with $a = 4$

Equilibrium points	Eigenvalues	Nature
$E1 = (3.4038,\ 0,\ 3.3915,\ 0)$	$\lambda_i = (75.1241,\ 2.0891 \pm 10.5252i,\ 0.1864)$	Unstable
$E2 = (-0.2622,\ 0,\ -0.2746,\ 0)$	$\lambda_i = (75.1243,\ 2.28240 \pm 10.09857i,\ -0.20029)$	Unstable

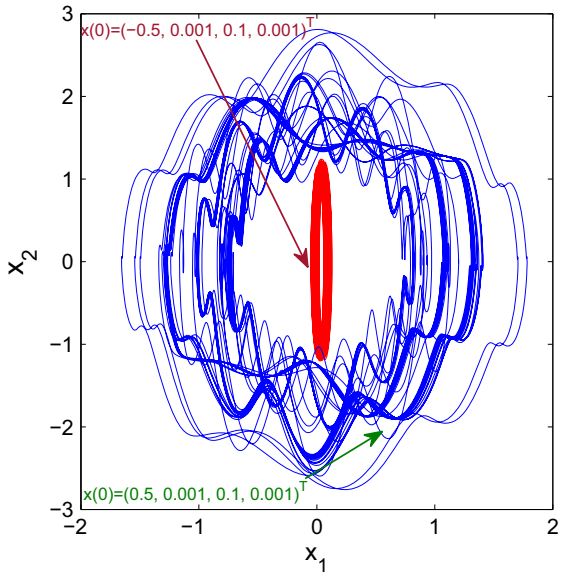

Fig. 14 Coexistence of chaotic orbits of system (12) with $x\,(0) = (\pm 0.5,\ 0.001,\ 0.1,\ 0.001)^{\mathrm{T}}$, $\triangle t = 0.01$, $a = 4$ and $3000 \leq T \leq 3500$

$$\begin{cases} \dot{x}_1 = x_2 \\ \dot{x}_2 = -p_1 \sin(x_1) - p_2 (x_1 - x_3) \\ \dot{x}_3 = x_4 \\ \dot{x}_4 = p_3 (x_1 - x_3) - p_4 x_4 + p_5\, a\, cos\,(2\pi f t)\,. \end{cases} \tag{14}$$

Two different subcases are considered with changes in the amplitude of the control input to show different chaotic behaviours in system (14). System (14) is a dissipative chaotic system whose divergence is $\nabla v = -p_4$. Thus, the volume of system (14) decays exponentially at a rate equal to p_4 with $p_4 > 0$. Therefore, there may exist attractor for system (14). System (14) is not invariant under the coordinate transformation and has asymmetry to its coordinate axes, plane and space.

6.1 Case 4(A): Control input ($u = 2.29\cos(2\pi f t)$)

Using this control input, system (14) with the original parameters exhibit transient chaotic behaviour when $x\,(0) = (0.1,\ 0.001,\ 0.1,\ 0.1)^{\mathrm{T}}$. Time response and phase portraits of system (14) are shown in Fig. 17. It is seen from Fig. 17a that system (14) has chaotic

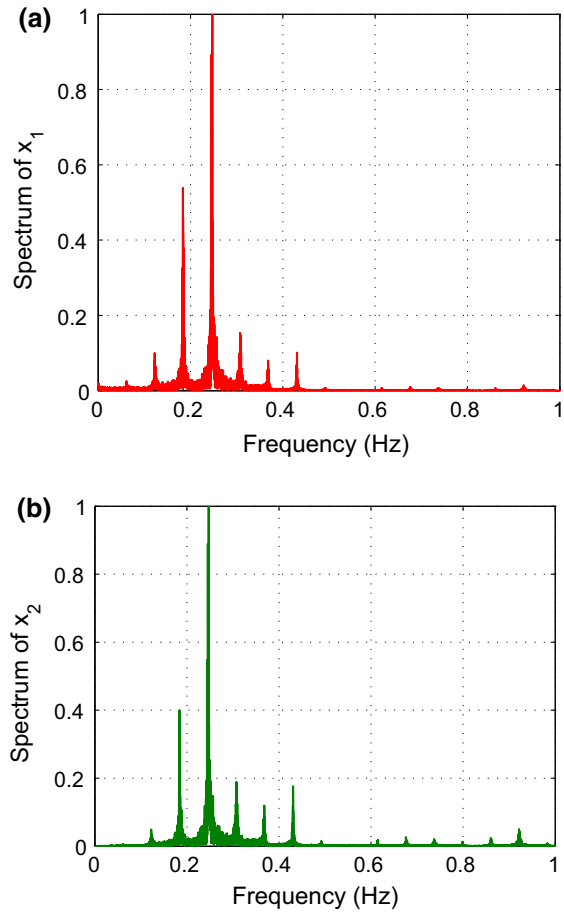

Fig. 15 Frequency spectra of system (12) with $x\,(0) = (0.5,\ 0.001,\ 0.1,\ 0.001)^{\mathrm{T}}$

behaviour during transient phase ($0 < T < 780$) and has a stable limit cycle for time $T > 780$. The transient chaotic and stable limit cycle behaviours of system (14) are shown in Figs. 17b, c, respectively. The transient chaotic behaviour of system (14) is analysed using other numerical tools like Lyapunov exponents and instantaneous phase plot.

6.1.1 Lyapunov exponents

Lyapunov exponents of system (14) are calculated to know the chaotic and periodic behaviours of system (14) for Case 4(A). Here, Wolf algorithm [78] is used to calculate Lyapunov exponents (LEs). The LEs of system (14) with $x\,(0) = (0.1, 0.001, 0.1, 0.1)^{\mathrm{T}}$, $\triangle t = 0.01$ and observation time $T = 1200$ are shown in Fig. 18. It is seen from Fig. 18 that the highest

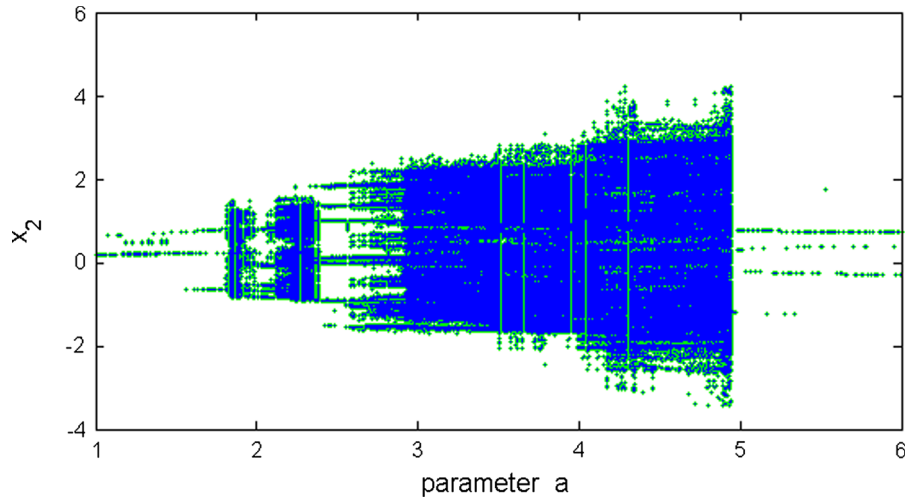

Fig. 16 Bifurcation diagram of system (12) with $x\,(0) = (0.5,\ 0.001,\ 0.1,\ 0.001)^{\mathrm{T}}$

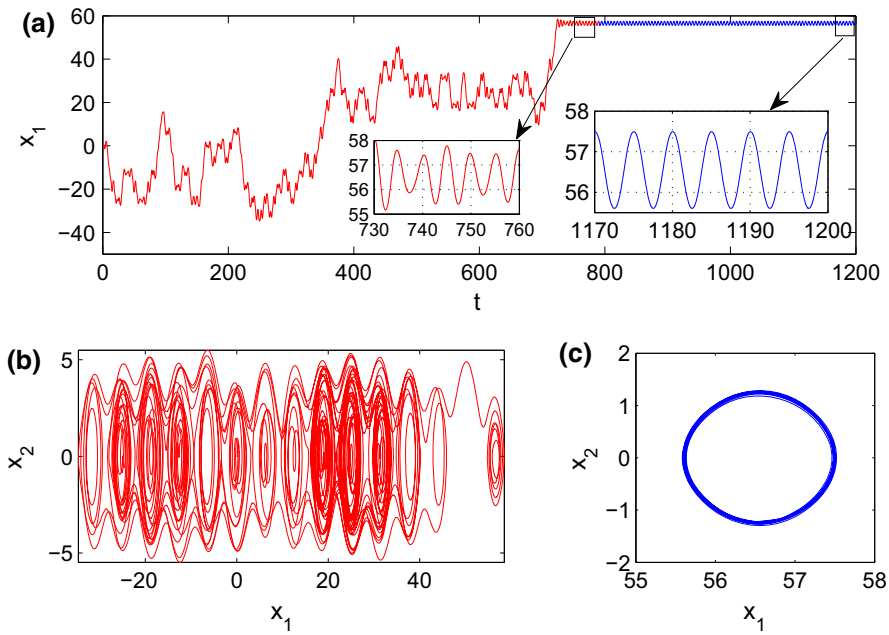

Fig. 17 Transient chaotic behaviour of Case 4(A) of system (14) with $x\,(0) = (0.1,\ 0.001,\ 0.1,\ 0.1)^{\mathrm{T}}$, $\triangle t = 0.01$: **a** time series, **b** transient chaotic orbit for $0 < T < 780$ and **c** stable limit cycle for $T > 780$

Lyapunov exponent is positive during transient chaotic region ($0 < T < 780$), and thus, the system has chaotic behaviour. However, the highest Lyapunov exponent is zero at $T > 780$, and hence, the system has limit cycle behaviour.

6.1.2 Instantaneous phase (IP)

Here, Hilbert transformation (HT) method [81] is used to calculate the instantaneous phase ($\emptyset_I$) in Case 4(A) of system (14). Suppose $s\,(t)$ is the complex form of a signal $x(t)$ in the form given as follows: [82],

$$s\,(t) = x\,(t) + \tilde{x}\,(t) = A(t)e^{i\emptyset_I(t)}, \tag{15}$$

with $A(t)$ and $\emptyset_I(t)$ as the amplitude and phase, respectively, of signal x(t), where $\tilde{x}\,(t)$is defined as

$$\tilde{x}\,(t) = \frac{1}{\pi} PV\left(\int_{-\infty}^{\infty} \frac{x(\tau)}{x(t-\tau)}\mathrm{d}\tau\right). \tag{16}$$

In (16), PV is the Cauchy principle component in HT. The instantaneous phase of a chaotic system increases monotonically with respect to time, whereas it remains constant for a periodic system. The instantaneous phase

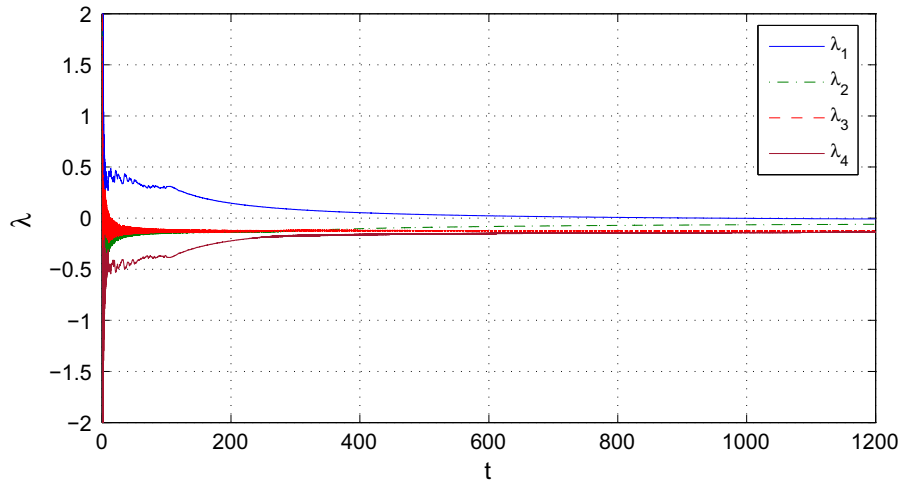

Fig. 18 Lyapunov exponents of Case 4(A) of system (14) with $x\,(0) = (0.1,\ 0.001,\ 0.1,\ 0.1)^{\mathrm{T}}$ and $\triangle t = 0.01$

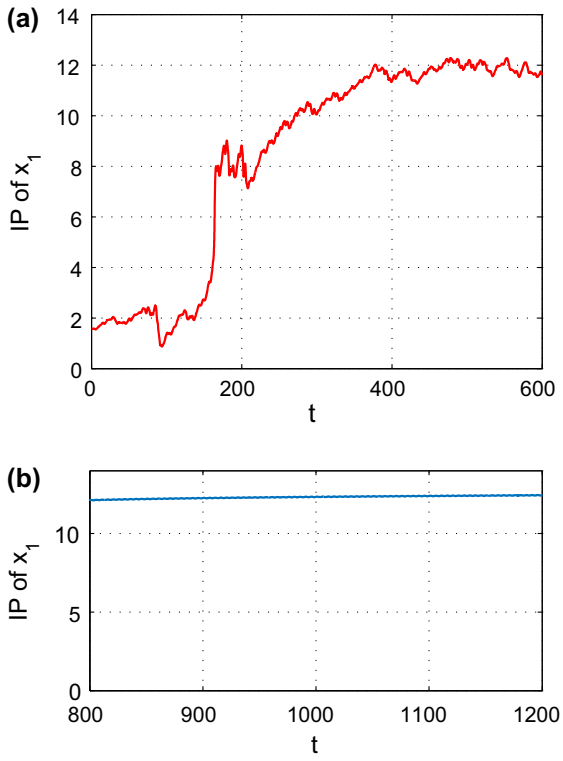

Fig. 19 Instantaneous phase (IP) of x_1 signal of Case 4(A) of system (14): **a** during transient chaotic region and **b** in stable limit cycle region

of x_1 signal in Case 4(A) of system (14) is shown in Fig. 19. It is seen from Fig. 19 that during transient chaotic region, the instantaneous phase of the signal $x_1(t)$ increases monotonically with time, whereas during limit cycle region, the instantaneous phase is almost constant.

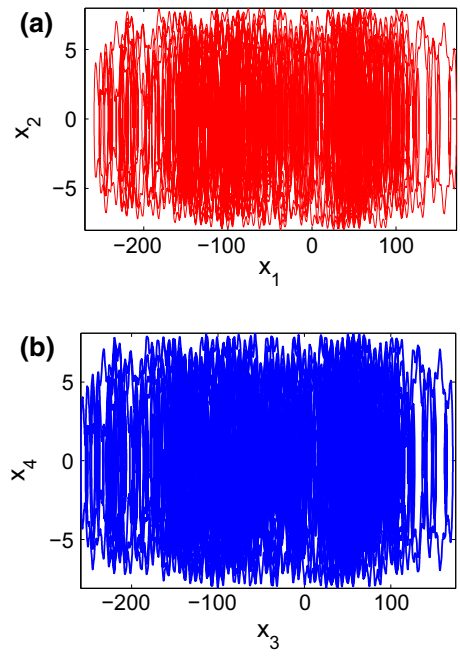

Fig. 20 Chaotic orbits of Case 4(B) of system (14) with $x\,(0) = (0.1,\ 0.001,\ 0.1,\ 0.001)^{\mathrm{T}}$, $\triangle t = 0.01$ and $T = 1000$

6.2 Case 4(B): Control input ($u = 4\cos(2\pi f t)$)

In this subcase, system (14) is chaotic and its chaotic orbits are shown in Fig. 20. Coexistence of chaotic orbits in Case 4(B) of system (14) is shown in Fig. 21. The chaotic orbits in Fig. 20 are generated with $T = 1000$ observation time and ignoring initial transient responses. The chaotic behaviour in Case 4(B) of system (14) is also validated by using Poincaré map. The

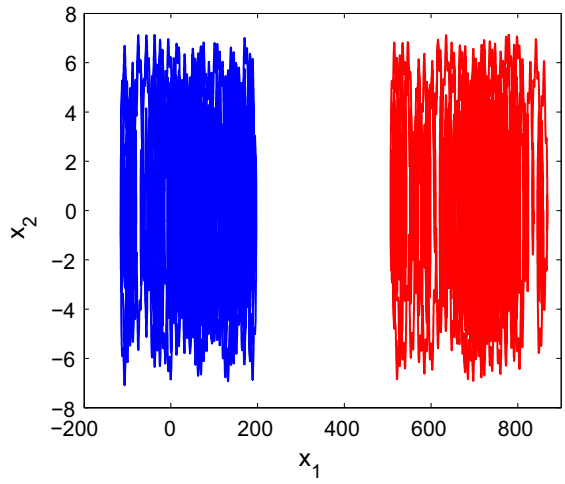

Fig. 21 Coexistence of chaotic orbits of Case 4(B) of system (14) with $x\,(0) = (\pm 0.1,\ 0.001,\ 0.1,\ 0.001)^{\mathrm{T}}$, $\triangle t = 0.01$ and $2500 < T < 3000$

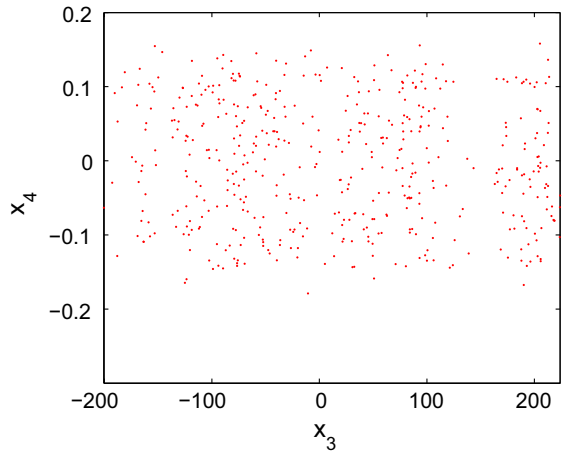

Fig. 22 Poincaré map of Case 4(B) of system (14) with $x_1 = 0$, $x\,(0) = (0.1,\ 0.001,\ 0.1,\ 0.001)^{\mathrm{T}}$, $\triangle t = 0.01$, across $x_3 - x_4$

Poincaré map is plotted about $x_1 = 0$ in $x_3 - x_4$ plane and is shown in Fig. 22. The random location of the dots in Fig. 22 indicates that Case 4(B) of system (14) has chaotic behaviour.

6.3 An inverse crisis route to chaos in (14)

It is seen in Case 4(A) and Case 4(B) that with the variation in amplitude of the control input, the responses of the SLFJ manipulator change. For smaller values of the amplitude of the control input u, system (14) has transient chaotic behaviour, and for larger values, the system has chaotic behaviour. Bifurcation diagram is plotted to know the variation of such changes. Bifurcation diagram with a variation of parameter a of system (14) is shown in Fig. 23. It is seen from Fig. 23 that system (14) has different dynamical behaviours like periodic and chaotic with the variation of amplitude a. The system has transient chaotic behaviour for initial values of parameter a and has chaotic behaviour for larger values of parameter a. Thus, the system has an inverse crisis route to chaos [82]. This indicates another interesting property of system (14). The periodic nature of system (14) with $a = 2$ is shown in Fig. 24.

6.4 Chaos validation of Case 4(B) using 0–1 test

The 0–1 test is used to classify the periodic and chaotic behaviours of a system. For a chaotic system, the outcomes of the 0–1 test are approximately equal to one, and for a periodic response, it is equal to zero. Here, the original dynamics is transformed into translation variable $(p_c\,(n)\,,\ q_c\,(n))$ and average growth rate of mean square displacement $(M_c(n))$ [83,84] is measured. The variables $(p_c\,(n)\,,\ q_c\,(n))$ are defined as

$$\begin{cases} p_c\,(n) = \sum_{j=1}^{n} x\,(j)\cos jc \\ q_c\,(n) = \sum_{j=1}^{n} x\,(j)\sin jc, \end{cases} \tag{17}$$

where c is an arbitrarily chosen variable in the range $(0-2\pi)$ and $x\,(j)$ is the time series of any state variable of the system. The phase variables $p_c\,(n)$ and $q_c\,(n)$ represent a random Brownian-like motion for a chaotic system, whereas the behaviour is a bounded motion for a periodic signal. The mean square displacement $M_c(n)$ is defined in (18) [83,84]

$$M_c(n) = \lim_{N\to\infty} \frac{1}{N} \sum_{k=1}^{N} \times \left\{ [p_c\,(k+n) - p_c(k)]^2 + [q_c\,(k+n) - q_c(k)]^2 \right\} \tag{18}$$

The $M_c\,(n)$ grows exponentially for the chaotic behaviour, whereas it varies periodically for a periodic behaviour. The asymptotic growth rate (k_c) is defined in (19) [83–85]

$$k_c = \lim_{n\to\infty} \frac{\log\ M_c(n)}{\log n}\ . \tag{19}$$

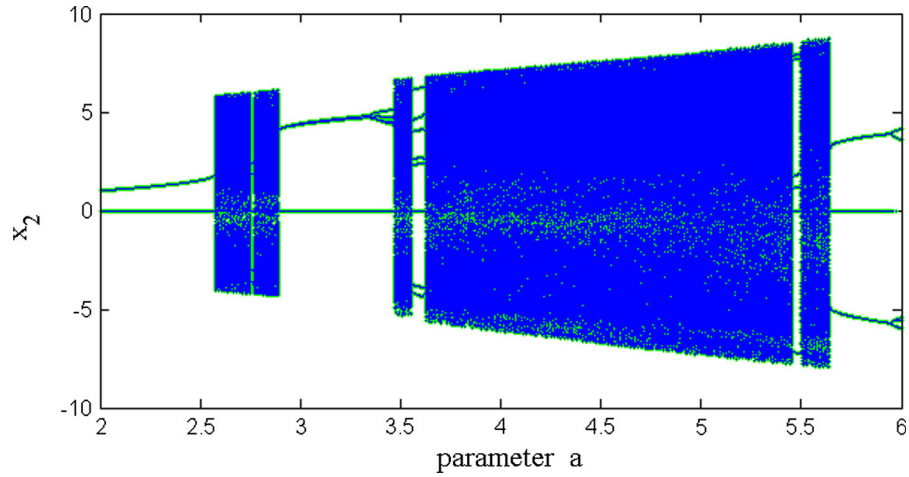

Fig. 23 Bifurcation diagram of system (14) by varying amplitude of control input with $x\,(0) = (0.1,\ 0.001,\ 0.1,\ 0.001)^{\mathrm{T}}$ and $\triangle t = 0.01$

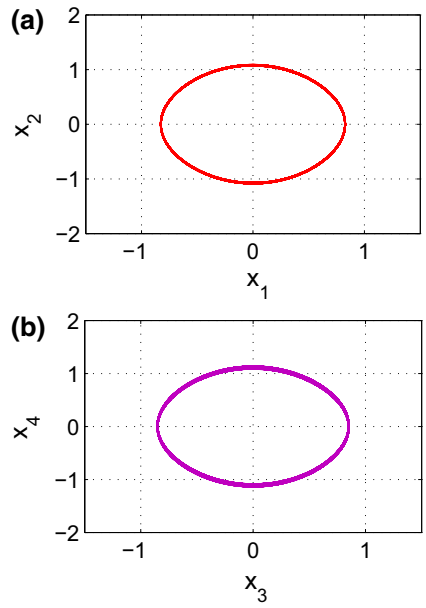

Fig. 24 Periodic orbits for system (14) when amplitude of control input is $a = 2$ with $x\,(0) = (0.1,\ 0.001,\ 0.1,\ 0.001)^{\mathrm{T}}$ and $\triangle t = 0.01$

The value of the growth rate for a chaotic signal is approximately equal to one and the same for a periodic signal approximately equals to zero. Phase plane of translation variables $(p_c,\ q_c)$, asymptotic growth rate (k_c) and mean square displacement $(M_c\,(n))$ in Case 4(B) of system (14) with initial conditions $x\,(0) = (0.1,\ 0.001,\ 0.1,\ 0.001)^{\mathrm{T}}$ are shown in Fig. 25. It is obvious from Fig. 25 that the phase plane across the translation variables $(p_c,\ q_c)$ is Brownian-like motion, asymptotic growth rate has constant one values and the mean square displacement $(M_c\,(n))$ grows monotonically. These all confirms that Case 4(B) of system (14) has chaotic behaviour. For Case 4(B), the system has $k = 0.9987 \approx 1$ which indicates the chaotic nature of the signal.

7 Circuit design and implementation of the SLFJ manipulator

The designed circuit of system (8) for Case 1(I) is shown in Fig. 26. The circuit is designed using NI Multisim 12 software. Several chaotic systems are implemented and verified using NI Multisim [86–90]. NI Multisim components are based on actual circuit components. Simulation results obtained using NI Multisim are in consistence with the actual circuit results [87]. The circuit (Fig. 26) of system (8) for Case 1(I) consists of four integration lines for four states of the system. The circuit consists of four capacitors $(C1, C2, C3, C4)$, 17 resistors, six op-amp (741) and two analog behavioural model (ABM) blocks. Here, ABM block is used for the implementation of sin and cos terms. The circuit equations corresponding to each state in Case 1(I) of system (8) can be written using Kirchhoff's law as:

$$\begin{cases} \dot{x}_1 = \frac{1}{RC1}\left[\frac{R}{R1}x_2\right] \\ \dot{x}_2 = \frac{1}{RC2}\left[-\frac{R}{R4}x_1 + \frac{R}{R5}x_3 - \frac{R}{R6}\sin(x_1)\right] \\ \dot{x}_3 = \frac{1}{RC3}\left[\frac{R}{R9}x_4\right] \\ \dot{x}_4 = \frac{1}{RC4}\left[\frac{R}{R13}x_1 - \frac{R}{R12}x_3 - \frac{R}{R15}x_4 + \frac{R}{R14}(3\cos(2\pi x_2))\right], \end{cases} \tag{20}$$

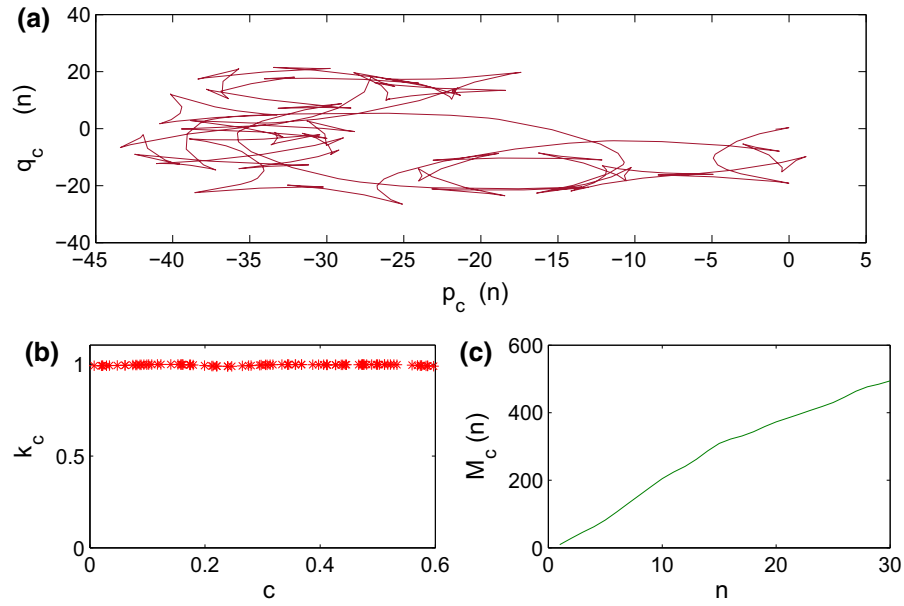

Fig. 25 0–1 test of x_2 signal of Case 4(B) of system (14) $x\,(0) = (0.01,\ 0.001,\ 0.001,\ 0.1)^{\mathrm{T}}$, $\triangle t = 1$: **a** phase plane between $p_c\,(n)$ and $q_c(n)$, **b** asymptotic growth rate (k_c) and **c** mean square displacement $M_c\,(n)$

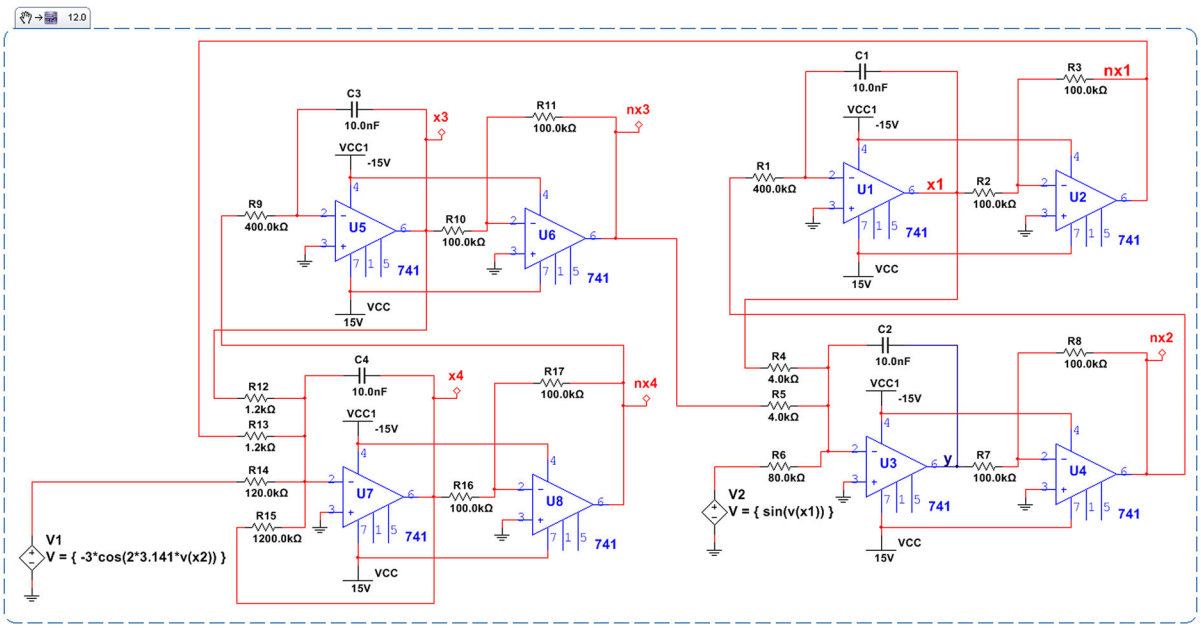

Fig. 26 Circuit implementation of Case 1(I) of system (8)

where the variables $x_1,\ x_2,\ x_3,\ x_4$ are the output of op-amp integrators $u1,\ u3,\ u5,\ u7$. Case 1(I) of system (8) is equivalent to (20) with $\tau = t/RC$, $R = 400$, $\frac{R}{p_1} = 80 = R6$, $\frac{R}{p_2} = 4 = R4 = R5$, $\frac{R}{p_3} = 1.25 = R12 = R13$, $\frac{R}{p_4} = 1200 = R15$, $\frac{R}{p_5} = 120 = R14$ and $a = 3$. Chaotic attractors in Case 1(I) of system (8) obtained using the circuit implementation are shown in Fig. 27. The circuit implementation of Case 1(II) and Case 1(III) is same as that of Case 1(I) except for some small changes in values of $C1 = C2 = C3 = C4 = 1.0\,nF$, $v1 = 4\cos(2\pi x_2)$ and $C1 = C2 = C3 = C4 = 1.0\,nF$, $v1 = 5\cos(2\pi x_2)$

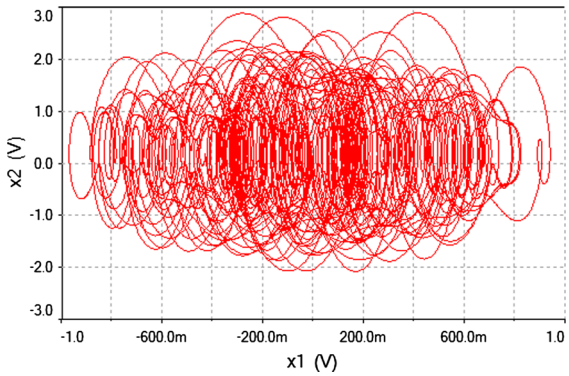

Fig. 27 Chaotic attractors in Case 1(I) of system (8) obtained using NI Multisim circuit implementation

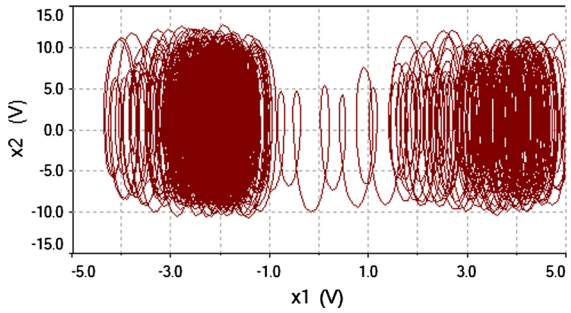

Fig. 28 Chaotic attractors in Case 1(II) of system (8) obtained using NI Multisim circuit implementation

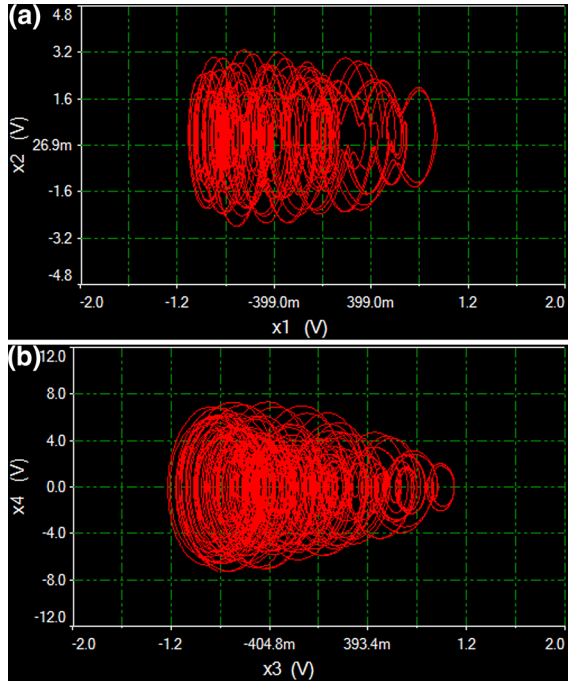

Fig. 29 Chaotic attractors for Case 2 obtained using NI Multisim circuit implementation

for Case 1(II) and Case 1(III), respectively. The chaotic attractors in Case 1(II) of system (8) obtained using the circuit implementation are shown in Fig. 28. Similarly, the circuit design of system (10) and (12) is same as in the Case 1(I) of system (8) which is shown in Fig. 26 but with the changes in $C1 = C2 = C3 = C4 = 10.0\,nF$, $v1 = 3\cos(x_2 - 0.5)\tanh(100(x_2 - 0.5))$ and $C1 = C2 = C3 = C4 = 1.0\,nF$, $v1 = 4\cos(2\pi(x_4 - 0.3))$, respectively, for system (10) and (12). Chaotic attractors of system (10) and (12) obtained using circuit implementation are shown in Figs. 29 and 30, respectively. It is observed from Fig. 20 that x_1 and x_3 states of Case 4(B) are approximately in the ranges of $[-300, 200]$ and $[-300, 200]$, respectively. Thus, the x_1 and x_3 states are scaled and the new system variables are defined as $u = \frac{x_1}{100}$, $v = x_2$, $z = \frac{x_3}{100}$, $w = x_4$. The circuit equations corresponding to each state of Case 4(B) with new variables can be written using Kirchhoff's law as:

$$\begin{cases} \dot{u} = \frac{1}{RC1}\left[\frac{R}{100R1}v\right] \\ \dot{v} = \frac{1}{RC2}\left[-100(\frac{R}{R4}u - \frac{R}{R5}z) - \frac{R}{R6}\sin(100u)\right] \\ \dot{z} = \frac{1}{RC3}\left[\frac{R}{100R9}w\right] \\ \dot{w} = \frac{1}{RC4}\left[\frac{1}{100}(\frac{R}{R13}u - \frac{R}{R12}z) \right. \\ \quad \left. - \frac{R}{R15}w + \frac{R}{R14}(a\cos(2\pi f t))\right]. \end{cases} \tag{21}$$

The circuit design in Case 4(B) of system (14) is shown in Fig. 31. Chaotic attractors for Case 4(B) obtained using circuit implementation are shown in Fig. 32. It is observed from Figs. 27, 28, 29, 30 and 32 that the results obtained by circuit implementation of systems (8), (10), (12) and (14) confirm the MATLAB simulation results in Figs. 4, 5, 11, 13 and 20, respectively.

8 Application of an SLFJ manipulator for a weak signal detection

In this section, an application of an SLFJ manipulator robot dynamics for detecting a weak signal is discussed. The non-autonomous manipulator dynamics defined in (14) is used for this purpose. Figure 23

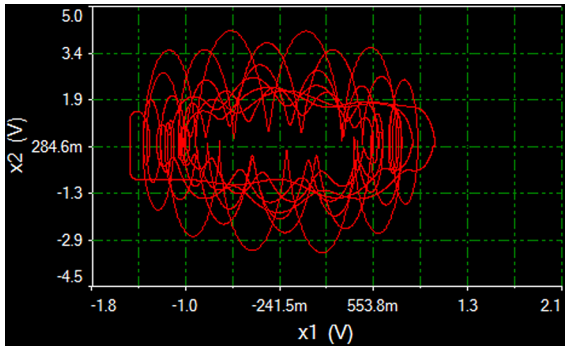

Fig. 30 Chaotic attractors for Case 3 obtained using NI Multisim circuit implementation

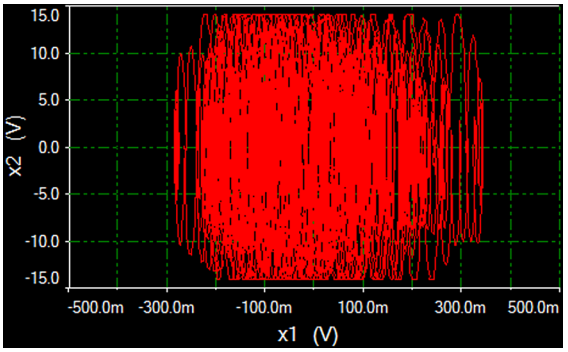

Fig. 32 Chaotic attractors in Case 4(B) of system (14) obtained using NI Multisim circuit implementation

and calculation show that when $a = 2.892565334$, system (14) is chaotic. When a is increased by a small value of 10^{-9} to $a = 2.892565335$, system (14) depicts periodic behaviour. Hence, we may consider $a_T = 2.892565334$ as the threshold value of the parameter of system (14). Thus, with the addition of a signal having amplitude equal to or greater than 10^{-9}, the system changes its state from chaotic to the large-scale periodic state. Therefore, system (14) can generate an alarm for the indication of a weak signal.

Application of system (14) for detecting a weak signal with various frequency can be achieved by frequency transformation as discussed below. Considering $t = w_0 T$, we can define as $x(t) = x(w_0 T)$; then, the transformed dynamics for (14) can be written as:

$$\begin{cases} \dot{x}_1 = w_0(x_2) \\ \dot{x}_2 = w_0(-p_1 \sin(x_1) - p_2(x_1 - x_3)) \\ \dot{x}_3 = w_0(x_4) \\ \dot{x}_4 = w_0(p_3(x_1 - x_3) - p_4 x_4 + p_5\, a\, \cos(w w_0 T)). \end{cases} \tag{22}$$

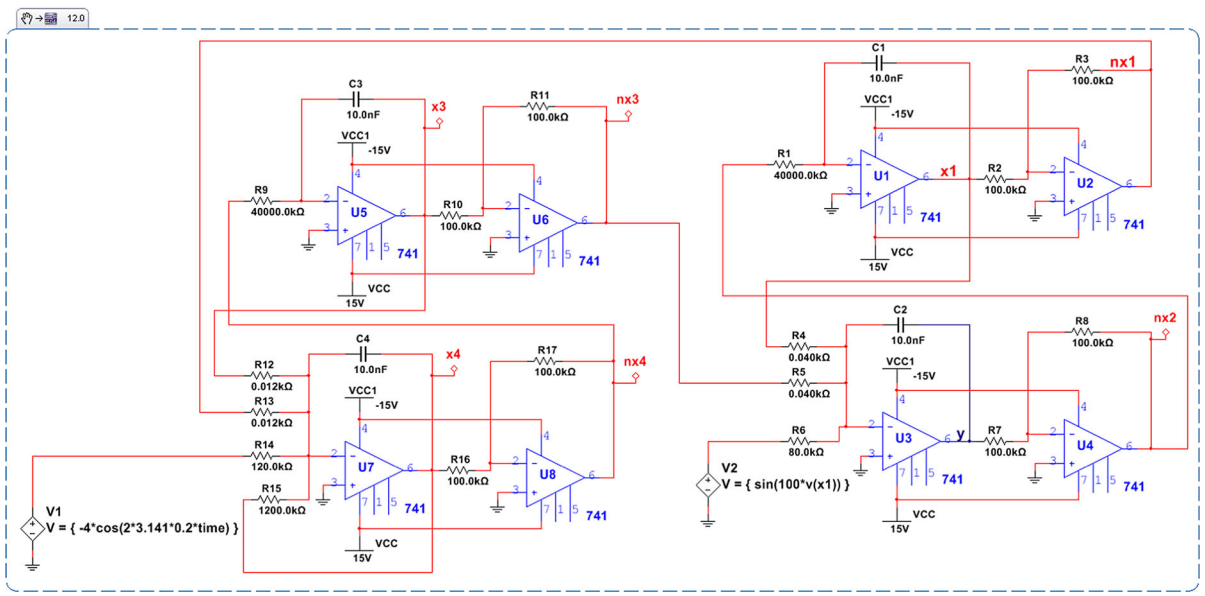

Fig. 31 Circuit implementation in Case 4(B) of system (14)

In order to detect a weak signal using system (22), an input (v) consists of the weak signal and noise is added. The expression is defined as:

$$\begin{cases} \dot{x}_1 = w_0(x_2) \\ \dot{x}_2 = w_0(-p_1 \sin(x_1) - p_2(x_1 - x_3)) \\ \dot{x}_3 = w_0(x_4) \\ \dot{x}_4 = w_0(p_3(x_1 - x_3) - p_4 x_4 \\ \qquad + p_5\, a\, \cos(w w_0 T) + v), \end{cases} \tag{23}$$

where $v = q \sin(w_0 T) + N(T)$, $q \sin(w_0 T)$ is the weak signal and $N(T)$ is the white Gaussian noise (WGN). The simulation results suggest that system (22) can detect the weak signal with very high frequency. The smallest signal-to-noise ratio (SNR) threshold can be achieved using (22) with $w_0 = 10^7$ rad/s, weak signal amplitude $q = 10^{-9}$, detection threshold $a_T = 2.892565335$ and noise power $P_N = 10^{-11}$, which is given as:

$$\begin{aligned} \mathrm{SNR(db)} &= 10 \log \frac{0.5(q)^2}{p_N} \\ &= 10 \log \frac{0.5(10^{-9})^2}{10^{-11}} = -73.010. \end{aligned} \tag{24}$$

9 Conclusions

In this paper, a single-link flexible joint manipulator dynamics is studied to show the occurrence of various chaotic behaviours. The generation of chaos in a SLFJ manipulator is shown for the first time to the best of authors' knowledge. The study has also added a new nature of equilibria in the classification of chaotic/hyperchaotic systems. A total of seven different cases/subcases are considered with the variation of control input. In three cases (five subcases), the closed-loop system is autonomous as the control input is considered as a partial state feedback control like joint velocity feedback and motor rotor velocity feedback. In the remaining case (two subcases), the open-loop system is non-autonomous since the control input is considered as a function of time. When the control input is considered as the joint velocity feedback, the system has (1) one stable spiral and one unstable saddle-node equilibrium points and (2) one marginally stable equilibrium point, in two subcases. When the control input is considered as the motor rotor velocity feedback, the SLFJ manipulator dynamics has two unstable equilibria in which one equilibrium point has index-4 spiral repellor nature. In the autonomous cases, the system depicts chaotic behaviour with single- and multi-scroll chaotic orbits. In non-autonomous cases, the system has (1) transient chaotic behaviour with a stable limit cycle at its steady state and (2) chaotic behaviour with a change in the amplitude of the control input. The system exhibits coexistence, (i.e. multi-stability) of chaotic orbits in all cases. Various tools are used to analyse the complex dynamics behaviour of the proposed SLFJ manipulator dynamics like phase portrait, time series plot, Poincaré map, bifurcation diagram, Lyapunov spectrum, frequency spectrum, instantaneous phase plot and 0–1 test. Chaotic nature of the proposed system is also validated using circuit implementation in NI Multisim software. The results obtained using the circuit have good agreement with the MATLAB simulation results. Finally, an application of proposed non-autonomous SLFJ manipulator for a weak signal detection is shown in the paper.

Acknowledgements Prof. N. V. Kuznetsov is supported by the RSF Project No. 14-21-00041p. This support is gratefully acknowledged.

References

1. Sprott, J.C.: Elegant Chaos, Algebraically Simple Chaotic Flows. World Scientific Publishing Co Pte Ltd, Singapore (2010)
2. Sprott, J.C.: Chaos and Time-Series Analysis. Oxford University Press, Oxford (2003)
3. Kuznetsov, N.V., Mokaev, T.N., Vasilyev, P.A.: Numerical justification of Leonov conjecture on Lyapunov dimension of Rossler attractor. Commun. Nonlinear Sci. Numer. Simul. **19**(4), 1027–1034 (2014)
4. Wei, Z., Pham, V.T., Kapitaniak, T., Wang, Z.: Bifurcation analysis and circuit realization for multiple-delayed Wang–Chen system with hidden chaotic attractors. Nonlinear Dyn. **85**(3), 1–16 (2016)
5. Wei, Z., Yu, P., Zhang, W., Yao, M.: Study of hidden attractors, multiple limit cycles from Hopf bifurcation and boundedness of motion in the generalized hyperchaotic Rabinovich system. Nonlinear Dyn. **82**(1–2), 31–141 (2015)
6. Lawande, Q., Ivan, B., Dhodapkar, S.: Chaos based cryptography: a new approach to secure communications. BARC Newslett. **258**, 258 (2005)
7. Banerjee, S., Kurths, J.: Chaos and cryptography: a new dimension in secure communications. Eur. Phys. J. Spec. Top. **223**, 1441–1445 (2014)

8. Banerjee, S., Mitra, M., Rondoni, L.: Applications of Chaos and Nonlinear Dynamics in Engineering, vol. 1. Springer, New York (2011)
9. Leonov, G.A., Kuznetsov, N.V., Vagaitsev, V.I.: Hidden attractor in smooth Chua systems. Phys. D Nonlinear Phenom. **241**, 1482–1486 (2012)
10. Leonov, G.A., Kuznetsov, N.V., Vagaitsev, V.I.: Localization of hidden Chuas attractors. Phys. Lett. A **375**, 2230–2233 (2011)
11. Leonov, G.A., Kuznetsov, N.V., Mokaev, T.N.: Homoclinic orbits, and self-excited and hidden attractors in a Lorenz-like system describing convective fluid motion. Eur. Phys. J. Spec. Top. **224**, 1421–1458 (2015)
12. Dudkowski, D., Jafari, S., Kapitaniak, T., Kuznetsov, N.V., Leonov, G.A., Prasad, A.: Hidden attractors in dynamical systems. Phys. Rep. **637**, 1–50 (2016)
13. Leonov, G.A., Kuznetsov, N.V.: Hidden attractors in dynamical systems: from hidden oscillations in Hilbert-Kolmogorov, Aizerman, and Kalman problems to hidden chaotic attractor in Chua circuits. Int. J. Bifurc. Chaos **23**, 1330002–130071 (2013)
14. Bragin, V.O., Vagaitsev, V.I., Kuznetsov, N.V., Leonov, G.A.: Algorithms for finding hidden oscillations in nonlinear systems. The Aizerman and Kalman conjectures and Chuas circuits. J. Comput. Syst. Sci. Int. **50**, 511–543 (2011)
15. Leonov, G.A., Kuznetsov, N.V., Kuznestova, O.A., Seledzhi, S.M., Vagaitsev, V.I.: Hidden oscillations in dynamical systems. Trans. Syst. Control. **6**, 1–14 (2011)
16. Leonov, G.A., Kuznetsov, N.V.: Algorithms for searching for hidden oscillations in the Aizerman and Kalman problems. Dokl. Math. **84**, 475–481 (2011)
17. Li, Z., Park, J.B., Joo, Y.H., Zhang, B.: Bifurcations and chaos in a permanent-magnet synchronous motor. IEEE Trans. Circuit Syst. I Fundam. Theory Appl. **49**, 383–387 (2002)
18. Gao, Y., Chau, K.T.: Hopf bifurcation and chaos in synchronous reluctance motor drives. IEEE Trans. Energy Convers. **19**, 296–302 (2004)
19. Kundu, S., Kar, U., Chakrabarty, K.: Co-existence of multiple attractors in the PWM controlled DC drives. Eur. Phys. J. Spec. Top. **222**, 699–709 (2013)
20. Sangrody, R.A., Nazarzadeh, J., Nikravesh, K.Y.: Bifurcation and Lyapunovs exponents characteristics of electrical scalar drive systems. IET Power Electron. **5**, 1236–1340 (2012)
21. Ge, Z.-M., Chang, C.-M.: Chaos synchronization and parameters identification of single time scale brushless DC motors. Chaos Solitons Fractals **20**, 883–903 (2004)
22. Leonov, G.A., Kuznetsov, N.V., Kiseleva, M.A., Solovyeva, E.P., Zaretskiy, A.M.: Hidden oscillations in mathematical model of drilling system actuated by induction motor with a wound rotor. Nonlinear Dyn. **77**, 277–288 (2014)
23. Yuefeng, G.: Chaos control algorithm for redundant robotic obstacle avoidance. Inf. Technol. J. **12**, 704–711 (2013)
24. Ge, Y.X.: The space redundant robotic manipulator chaotic motion dynamics control algorithm. Sens. Transducers **175**, 27–31 (2014)
25. Duarte, M., Fernando, B.M., Machado, J.A.T.: Chaos dynamics in the trajectory control of redundant manipulators. In: Proceedings of the IEEE International Conference on Robotics and Automation, ICRA 2000, pp. 4109–4114 (2000)
26. Sofroniou, A., Bishop, S.: Dynamics of a parametrically excited system with two forcing terms. Mathematics **2**, 172–195 (2014)
27. Luo, A.C.J., Guo, Y.: Periodic motions to chaos in pendulum. Int. J. Bifurc. Chaos. **26**, 1650159–165070 (2016)
28. Kiseleva, M.A., Kuznetsov, N.V., Leonov, G.A.: Hidden attractors in electromechanical systems with and without equilibria. IFAC Papers OnLine **49**, 051–055 (2016)
29. Zang, X., Iqbal, S., Zhu, Y., Liu, X., Zhao, J.: Applications of chaotic dynamics in robotics. Int. J. Adv. Robot. Syst. **13**(2), 1–17 (2016)
30. Lochan, K., Roy, B.K., Subudhi, B.: A review on two-link flexible manipulators. Annu. Rev. Control **42**, 346–367 (2016)
31. Liu, H., Zhaohui, L., Zhang, L.: Control chaos in a spatially redundant manipulator with flexible Link. In: 12th IFToMM World Congress Besanon, Besanon (2007)
32. Dwivedy, S.K., Kar, R.C.: Nonlinear dynamics of a cantilever beam carrying an attached mass with 1:3:9 internal resonances. Nonlinear Dyn. **31**, 49–72 (2003)
33. Zhihua, F., Haiyan, H.: Principal parametric and three-to-one internal resonances of flexible beams undergoing a large linear motion. Acta Mech. Sin. **19**, 355–364 (2003)
34. Dwivedy, S.K., Kar, R.C.: Simultaneous combination and 1:3:5 internal resonances in a parametrically excited beam-mass system. Int. J. Non. Linear. Mech. **38**, 585–596 (2003)
35. Pratiher, B., Dwivedy, S.K.: Nonlinear vibration of a magneto-elastic cantilever beam with tip mass. J. Vib. Acoust. **131**, 21011 (2009)
36. Hamed, Y.S., Elagan, S.K.: On the vibration behavior study of a nonlinear flexible composite beam under excitation forces via nonlinear active vibration controller. Int. J. Basic Appl. Sci. **13**, 09–18 (2013)
37. Sadri, M., Younesian, D., Esmailzadeh, E.: Nonlinear harmonic vibration and stability analysis of a cantilever beam carrying an intermediate lumped mass. Nonlinear Dyn. **84**, 1–16 (2016)
38. Dupac, M., Beale, D.G.: Dynamic analysis of a flexible linkage mechanism with cracks and clearance. Mech. Mach. Theory. **45**, 1909–1923 (2010)
39. Dwivedy, S.K., Kar, R.C.: Non-linear dynamics of a slender beam carrying a lumped mass under principal parametric resonance with three-mode interactions. Int. J. Non. Linear. Mech. **36**, 927–945 (2001)
40. Dwivedy, S.K., Kar, R.C.: Simultaneous combination, principal parametric and internal resonances in a slender beam with a lumped mass: three-mode interactions. J. Sound Vib. **242**, 27–46 (2001)
41. Dwivedy, S., Kar, R.: Dynamics of a slender beam with an attached mass under combination parametric and internal resonances, Part II: periodic and chaotic responses. J. Sound Vib. **222**, 281–305 (1999)
42. Feng, Z.H., Lan, X.J., Zhu, X.D.: Principal parametric resonances of a slender cantilever beam subject to axial narrow-band random excitation of its base. Int. J. Non. Linear. Mech. **42**, 1170–1185 (2007)
43. Yin, C., Zhong, S.-M., Chen, W.-F.: Design of sliding mode controller for a class of fractional-order chaotic systems.

Commun. Nonlinear Sci. Numer. Simul. **17**(1), 356–366 (2012)
44. Yin, C., Cheng, Y., Chen, Y.Q., Stark, B., Zhong, S.: Adaptive fractional-order switching-type control method design for 3D fractional-order nonlinear systems. Nonlinear Dyn. **82**(1–2), 39–52 (2015)
45. Yin, C., Cheng, Y., Zhong, S.-M., Bai, Z.: Fractional-order switching type control law design for adaptive sliding mode technique of 3D fractional-order nonlinear systems. Complexity **21**(6), 363–373 (2015)
46. Rostami Kandroodi, M., Farivar, F., Zamani Pedram, M., Aliyari Shoorehdeli, M.: Variable structure control and anti-control of flexible joint manipulator with experimental validation. In: Proceedings of the 2011 IEEE International Conference Mechatronics (ICM), IEEE, Istanbul, pp. 294–299 (2011)
47. Kandroodi, M.R., Farivar, F., Shoorehdeli, M.A.: Lyapunov based control of flexible joint manipulator with experimental validation by using chaotic gyroscope synchronization. Int. J. Mech. Syst. Eng. **2**, 169–175 (2012)
48. Zamani, M., Aliyari, M., Farivar, F.: Hybrid concepts of the control and anti-control of flexible joint manipulator. Int. J. Robot. **2**, 35–44 (2011)
49. Wang, F., Bajaj, A.K.: Nonlinear dynamics of a three-beam structure with attached mass and three-mode interactions. Nonlinear Dyn. **62**, 461–484 (2010)
50. Farahan, S.B., Ghazavi, M., Rahmanian, S.: Nonlinear dynamic analysis of a four-bar mechanism having revolute joint with clearance. J. Theor. Appl. Vib. Acoust. **2**, 91–106 (2016)
51. Pomares, J., Perea, I., Jara, C.A., Garca, G.J., Torres, F.: Dynamic visual servo control of a 4-axis joint tool to track image trajectories during machining complex shapes. Robot. Comput. Integr. Manuf. **29**, 261–270 (2013)
52. de la Fraga, L.G., Tlelo-Cuautle, E.: Optimizing the maximum Lyapunov exponent and phase space portraits in multi-scroll chaotic oscillators. Nonlinear Dyn. **76**(2), 503–1515 (2014)
53. Carbajal-Gmez, V.H., Tlelo-Cuautle, E., Fernndez, F.V., de la Fraga, L.G., Snchez-Lpez, C.: Maximizing Lyapunov exponents in a chaotic oscillator by applying differential evolution. Int. J. Nonlinear Sci. Numer. Simul. **15**(1), 11–17 (2014)
54. Pham, V.T., Volos, C., Jafari, S., Kapitaniak, T.: Coexistence of hidden chaotic attractors in a novel no-equilibrium system. Nonlinear Dyn. **87**(3), 2001–2010 (2016)
55. Pham, V.T., Vaidyanathan, S., Volos, C., Jafari, S., Kingni, S.T.: A no-equilibrium hyperchaotic system with a cubic nonlinear term. Optik **127**, 3259–3265 (2016)
56. Singh, J.P., Roy, B.K.: Analysis of an one equilibrium novel hyperchaotic system and its circuit validation. Int. J. Control Theory Appl. **8**, 1015–1023 (2015)
57. Wei, Z., Zhang, W.: Hidden hyperchaotic attractors in a modified Lorenz–Stenflo system with only one stable equilibrium. Int. J. Bifurc. Chaos. **24**, 1450127–1450132 (2014)
58. Bao, B.C., Li, Q.D., Wang, N., Xu, Q.: Multistability in Chuas circuit with two stable node-foci. Chaos Interdiscip. J. Nonlinear Sci. **26**, 43111–43120 (2016)
59. Singh, J.P., Roy, B.K.: A novel asymmetric hyperchaotic system and its circuit validation. Int. J. Control Theory Appl. **8**, 1005–1013 (2015)
60. Chen, Y., Yang, Q.: Dynamics of a hyperchaotic Lorenz-type system. Nonlinear Dyn. **77**, 569–581 (2014)
61. Yang, Q., Liu, Y.: A hyperchaotic system from a chaotic system with one saddle and two stable node-foci. J. Math. Anal. Appl. **360**, 293–306 (2009)
62. Tang, L., Zhao, L., School, Q.Z.: A novel four-dimensional autonomous hyperchaotic system ICAIC Part III, vol. 2011. Springer, Berlin (2011)
63. Li, Q., Zeng, H., Li, J.: Hyperchaos in a 4D memristive circuit with infinitely many stable equilibria. Nonlinear Dyn. **79**, 2295–2308 (2014)
64. Li, C., Sprott, J.C., Thio, W.: Bistability in a hyperchaotic system with a line equilibrium. J. Exp. Theor. Phys. **118**, 494–500 (2014)
65. Singh, J.P., Roy, B.K.: A Novel hyperchaotic system with stable and unstable line of equilibria and sigma shaped Poincare map. IFAC PapersOnLine **49**, 526–531 (2016)
66. Zhang, H., Li, Z.: Research on nonlinear dynamics of two-degrees-of-freedom robot. In: Xang, C., et al. (eds.) ICIRA, pp. 420–426. Springer, Berlin (2008)
67. Ravishankar, A., Ghosal, A.S.: Nonlinear dynamics and chaotic in feedback controlled two and three degree of freedom robot. Int. J. Rob. Res. **18**, 93–108 (1999)
68. Spong, M.W., Hutchinson, S., Vidyasagar, M.: Robot Modeling and Control, 1st edn. Wiley, New York (2002)
69. Thoma, M., Allgwer, F., Morari, M.: Robot Motion and Control. Scientific Publishing Services Pvt. Ltd, Chennai (2009)
70. Spong, M.W.: Adaptive control of flexible joint manipulators. Syst. Control Lett. **13**, 15–21 (1989)
71. Shen, C., Yu, S., Lu, J., Chen, G.: Designing hyperchaotic systems with any desired number of positive Lyapunov exponents via a simple model. IEEE Trans. Circuits Syst. I Regul. Pap. **61**(8), 2380–2389 (2014)
72. Shen, C., Yu, S., Lu, J., Chen, G.: A systematic methodology for constructing hyperchaotic systems with multiple positive Lyapunov exponents and circuit implementation. IEEE Trans. Circuits Syst. I Reg. Pap. **61**, 854–864 (2014)
73. Ma, J., Wu, X., Chu, R., Zhang, L.: Selection of multi-scroll attractors in Jerk circuits and their verification using Pspice. Nonlinear Dyn. **76**(4), 1951–1962 (2014)
74. Chen, J.L.G.: Generating multiscroll chaotic attractors: theories, methods and applications. Int. J. Bifurc. Chaos **16**(4), 775–858 (2006)
75. Jafari, S., Pham, V.-T., Kapitaniak, T.: Multiscroll chaotic sea obtained from a simple 3D system without equilibrium. Int. J. Bifurc. Chaos **26**(2), 1650031–1650036 (2016)
76. Zhang, H., Liu, X., Shen, X., Liu, J.: Chaos entanglement: a new approach to generate chaos. Int. J. Bifurc. Chaos **23**(5), 1330014–1330031 (2013)
77. Sahab, A.R., Modabbernia, M.R.: Backstepping method for a single-link flexible-joint manipulator using genetic algorithm. Int. J. Innov. Comput. Inf. Control. **7**, 4161–4170 (2011)
78. Wolf, A., Swift, J.B., Swinney, H.L., Vastano, J.A.: Determining Lyapunov exponents from a time series. Physica D **16**, 285–317 (1985)
79. Singh, J.P., Roy, B.K.: The nature of Lyapunov exponents is $(+, +, -, -)$. Is it a hyperchaotic system? Chaos Solitons Fractals **92**, 73–85 (2016)

80. Leonov, G.A., Kuznetsov, N.V.: Time-varying linearization and the Perron effects. Int. J. Bifurc. Chaos. **17**, 1079–1107 (2007)
81. Sabarathinam, S., Thamilmaran, K.: Transient chaos in a globally coupled system of nearly conservative Hamiltonian Duffing oscillators. Chaos Solitons Fractals **73**, 129–140 (2015)
82. Singh, J.P., Roy, B.K.: Crisis and inverse crisis route to chaos in a new 3-D chaotic system with saddle, saddle foci and stable node foci nature of equilibria. Optik **127**, 11982–12002 (2016)
83. Gottwald, B.G.A., Melbourne, I.: A new test for chaos in deterministic systems. Proc. Math. Phys. Eng. Sci. **460**, 603–611 (2004)
84. Gottwald, G.: On the implementation of the 0–1 test for chaos. Arxiv Prepr. arXiv:0906.1418. vol. 1367, pp. 1–22 (2009)
85. Sabarathinam, S., Thamilmaran, K., Borkowski, L., Perlikowski, P., Brzeski, P., Stefanski, A., et al.: Transient chaos in two coupled, dissipatively perturbed Hamiltonian Duffing oscillators. Commun. Nonlinear Sci. Numer. Simul. **18**, 3098–3107 (2013)
86. Xiong, L., Lu, Y.-J., Zhang, Y.-F., Zhang, X.-G., Gupta, P.: Design and hardware implementation of a new chaotic secure communication technique. PLoS ONE **11**(8), 1–19 (2016)
87. Zhang, R.-X., Yang, S.-P.: Adaptive synchronisation of fractional-order chaotic systems. Chin. Phys. B **19**(2), 1–7 (2010)
88. Lao, S.-K., Tam, L.-M., Chen, H.-K., Sheu, L.-J.: Hybrid stability checking method for synchronization of chaotic fractional-order systems. Abstr. Appl. Anal. **2014**, 1–11 (2014)
89. Kenfack, G., Tiedeu, A.: Secured transmission of ECG signals: numerical and electronic simulations. J. Signal Inf. Process. **04**(02), 158–169 (2013)
90. Chen, D., Liu, C., Wu, C., Liu, Y., Ma, X., You, Y.: A new fractional-order chaotic system and its synchronization with circuit simulation. Circuits Syst. Signal Process. **31**(5), 1599–1613 (2012)